

Supporting Information

Unraveling mechanistic insights into covalent organic frameworks for highly efficient sequestration of organic iodides from simulated nuclear waste

Sahel Fajal,^a Dipanjan Majumder,^a Writakshi Mandal,^a Sumanta Let,^a Gourab K. Dam,^a Mandar M. Shirolkar^{b,c} and Sujit K. Ghosh^{*a,d}

^aDepartment of Chemistry, Indian Institute of Science Education and Research (IISER) Pune, Dr. Homi Bhaba Road, Pashan, Pune 411008, India. Phone: +91 20 2590 8076

^bAdvanced Bio-Agro Tech Pvt. Ltd, Baner, Pune 411045, India.

^cNorel Nutrient Bio-Agro Tech Pvt. Ltd, Baner Pune 411045 India

^dCentre for Water Research (CWR), Indian Institute of Science Education and Research (IISER) Pune, Dr. Homi Bhaba Road, Pashan, Pune 411008, India.

Corresponding author. E-mail: sghosh@iiserpune.ac.in

Table of Contents

Section S1:	Page S3-S4
Materials, General Characterization and Physical Measurements	
Section S2:	Page S5-S10
Detail Synthetic Procedures for Synthetic Preparation	
Section S3:	Page S11-S13
Experimental Section	
Section S4:	Page S14-S14
Theoretical Calculation and Simulation Studies	
Section S5:	Page S15-S29
Structural Characterizations of the COFs	
Section S6:	Page S30-S32
Organic Iodide Capture Studies	
Section S7:	Page S33-S37
Chemical Stability Test and CH ₃ I Adsorption Study	
Section S8:	Page S38-S49
Post CH ₃ I Adsorption Characterizations	
Section S9:	Page S50-S68
Organic Dyes Adsorption Study	
Section S10:	Page S69-S69
References	

Section S1: Materials, General Characterizations and Physical Measurements

S1.1. Materials: All the reagents, starting materials and solvents were commercially purchased from Sigma-Aldrich, TCI Chemicals and spectrochem depending on their availability and used without further purification. 1,3,5-tris-(4-aminophenyl)-benzene was purchased from TCI chemicals.

S1.2. Safety Note: Methyl iodide and ethyl iodide vapor is toxic in nature and proper protective gear (masks, gloves) is always to be used. The organic iodide capture protocol described in this report that uses acid (in dynamic sorption) in a packed tube at high temperature must be carried out under strict safety precautions.

S1.3. General Characterizations and Physical Measurements:

S1.3.1. Powder X-ray diffraction (PXRD): Powder X-ray diffraction (PXRD) experiments were performed on a Bruker D8 Advanced X-ray diffractometer at room temperature using Cu K α radiation ($\lambda = 1.5406 \text{ \AA}$) at a scan speed of $0.5 \text{ }^\circ \text{ min}^{-1}$ and a step size of 0.01° in 2θ .

S1.3.2. Fourier transform infrared spectroscopy (FT-IR): The FT-IR spectra were acquired by using Bruker Optics ALPHA-II spectrophotometer using KBr pellet in $500\text{-}4000 \text{ cm}^{-1}$ range. The FT-IR data are reported with a wave number (cm^{-1}) scale in $500\text{-}4000 \text{ cm}^{-1}$ range.

S1.3.3. Thermogravimetric analysis (TGA): Thermogravimetric analyses were recorded on Perkin-Elmer STA 6000 TGA analyzer by heating the samples from 40 to $800 \text{ }^\circ\text{C}$ under N_2 atmosphere with a heating rate of $10 \text{ }^\circ\text{C min}^{-1}$.

S1.3.4. Solid-state nuclear magnetic resonance (NMR) spectroscopy: Solid-state ^{13}C cross-polarization-magic angle spinning (CP-MAS) spectra were conducted on a Bruker 500 MHz NMR spectrometer with a CP-MAS probe. Carbon chemical shifts are expressed in parts per million (δ scale).

S1.3.5. X-ray photoelectron spectroscopy (XPS): As-obtained powder samples was stuck to conductive paste and then measured by X-ray photoelectron spectroscopy using K-Alpha+model (Thermo Fischer Scientific, UK) with Al K α source.

S1.3.6. Nitrogen adsorption-desorption isotherm measurements: N_2 gas adsorption-desorption measurements were performed using BelSorp-Max instrument (Bel Japan). Prior to adsorption

measurements, the activated samples were heated at 120 °C under vacuum for 12 hours using BelPrepvacII.

S1.3.7. Field emission scanning electron microscopy (FESEM): The morphology of the materials was recorded with a Zeiss Ultra Plus field-emission scanning electron microscope (FESEM) with an integral charge compensator and embedded EsB and AsB detectors (Oxford X-max instruments 80 mm² (Carl Zeiss NTS, GmbH). The samples were sputter-coated with a 5-10 nm Au film to reduce charging. The elemental analysis was carried out using voltage of 15 KV equipped with an EDX detector. Data acquisition was performed with an accumulation time of >600s.

S1.3.8. Transmission electron microscopy (TEM): TEM, High-resolution TEM imaging and STEM-EDS were performed on the HRTEM (JEM-2200FS, JEOL) operating at acceleration voltage of 200 kV. For TEM analysis, all the samples were dispersed in isopropanol (0.5 mg/mL) and sonicated for 15 min. Then, the samples were left for 2 min, and the upper part of the solution was taken for preparing TEM samples on a lacey carbon-coated copper grid (Electron Microscopy Science, 200 mesh).

S1.3.9. Zeta potential: Zeta potential measurements were performed on Anton Paar Litesizer 500 series instrument. Measurement cell: Omega cuvette Mat. No. 155765, Target temperature 25.0 °C, Equilibration time – (Series parameter), Henry factor 1.1 (Other), Adjusted voltage (Automatic Mode), Number of runs 20, Solvent – water.

S1.3.10. UV-visible absorption spectra: UV-vis absorption studies were performed on a Shimadzu UV 3600 UV/vis spectrophotometer in an optical quartz cuvette (10 mm path length) over the entire range of 200-800 nm.

Section-S2: Detailed procedures for synthetic preparation

S2.1. Synthesis of 2,4,6-triformyl phenol (TFP) or 2-hydroxybenzene-1,3,5-tricarbaldehyde:

TFP was synthesized by following a previously reported procedure.^[1] A mixture of 6.9 g (65 mmol) of phenol was stirred with 70 mL of trifluoro acetic acid (TFA) and 20.1 g (143 mmol) of Hexamethylenetetramine (HMTA) at ~125 °C for about 20 h. After that, the reaction mixture was then heated to 148-150 °C and held at that temperature for 3 hours. Thereafter, the mixture was cooled to ~120 °C, and treated with 100 mL of 3N HCl, and then heated at ~100 °C for half an hour, then cooled to room temperature slowly by overnight. The resulting mixture were then filtered in a glass frit and washed with water to give a brown crude powder. The brown powders were then recrystallized from DMF and the needle shaped crystals were obtained as final product.

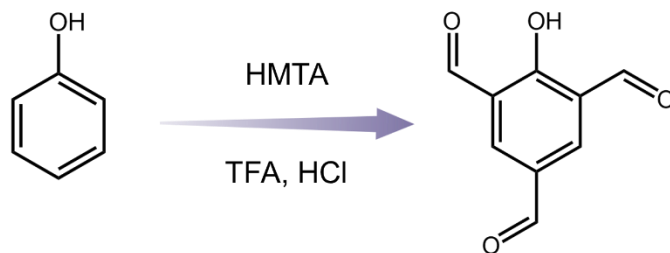


Figure-S1: Synthesis scheme of 2-hydroxybenzene-1,3,5-tricarbaldehyde.

S2.2. Synthesis of 4,4',4''-(pyridine-2,4,6-triyl)trianiline from 2,4,6-tris(4-nitrophenyl)pyridine:

4,4',4''-(pyridine-2,4,6-triyl)trianiline was synthesized by following a previously reported procedure.^[2] At first 2,4,6-tris(4-nitrophenyl)pyridine was synthesized.^[2] Briefly, 10 mmol of 4-Nitrobenzaldehyde and 20 mmol of 4-Nitroacetophenone were dissolved in 25 ml of acetic acid. Then 10 g of ammonium acetate was added to this mixture and refluxed at 110 °C for 3 hours. A dark red precipitate was filtered and washed with acetic acid and cold ethanol. After dried at ~80 °C, this dark red crude product was found as 2,4,6-tris(4-nitrophenyl)pyridine, which was further used in the next step for amine preparation.

In this step, 1.5 g of above 2,4,6-tris(4-nitrophenyl)pyridine was dissolved in 20 ml EtOH. Next, about 60 mg of ferric chloride hexahydrate and 200 mg of activated carbon were added to this solution and heated under reflux conditions for 30 mins. To this, 4 ml of hydrazine hydrate in 4 ml EtOH was added

dropwise and the mixture was refluxed for 12 hours. Thereafter, the mixture was filtered as hot and the filtrate was poured in excess distilled water. A white yellow precipitate with high yield was appeared, which was filtered, washed with water and dried at 60°C overnight.

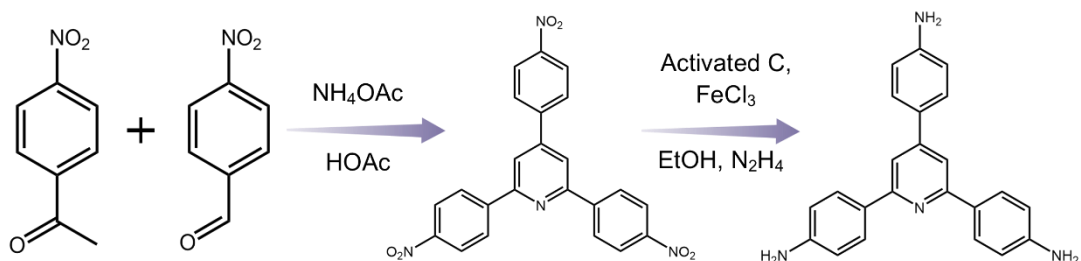


Figure-S2: Synthesis scheme of 4,4',4''-(pyridine-2,4,6-triyl)trianiline.

S2.3. Synthesis of 2,4,6-tris(4-aminophenyl)-1,3,5-triazine: 2,4,6-tris(4-aminophenyl)-1,3,5-triazine was synthesized from 4-aminobenzonitrile via an acid catalyzed trimerisation reaction by following a previously reported protocol.^[3] In a typical synthesis 4-aminobenzonitrile (591 mg, 5.0 mmol) was mixed with ~35 ml of chloroform taken in a dry RB (25 ml) and then 5.0 ml of triflic acid was added slowly at 0 °C and stirred under an inert atmosphere for 3 days. After that, the reaction mixture was gently poured into a beaker containing crushed ice-water and neutralized by 2M NaOH solution to afford yellow colored precipitate. This precipitate was filtered and washed with distilled water and dried at 60 °C overnight to get pure product.

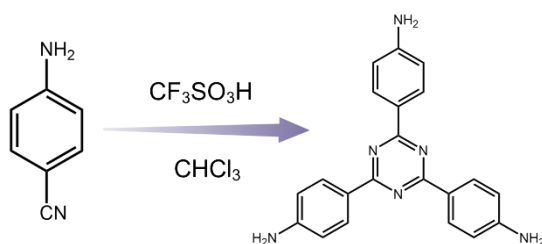


Figure-S3: Synthesis scheme of 2,4,6-tris(4-aminophenyl)-1,3,5-triazine.

S2.4. Synthesis of 5,5',5''-(1,3,5-triazine-2,4,6-triyl)tris(pyridin-2-amine): 5,5',5''-(1,3,5-triazine-2,4,6-triyl)tris(pyridin-2-amine) was synthesized from 6-Amino-3-pyridinecarbonitrile via an acid catalyzed trimerisation reaction by following a previously reported procedure.^[4] In a typical synthesis, 1.544 g (13.076 mmol) 6-Amino-3-pyridinecarbonitrile was taken in a round

bottom flask at $-20\text{ }^{\circ}\text{C}$. Then 8 mL of triflic acid ($\text{CF}_3\text{SO}_3\text{H}$) was added drop wise for 20 minutes. The resulting mixture was stirred for 24 h at room temperature in an inert atmosphere. Subsequently, the reaction mixture was quenched with distilled water and was neutralized by adding 2M NaOH solution until the pH was 7. At this pH, a pale yellow precipitate was observed which with further increase in pH it turns white. This white precipitate was filtered off and washed several times with distilled water. Next, the crude product was dried at $60\text{ }^{\circ}\text{C}$ overnight to get the final product.

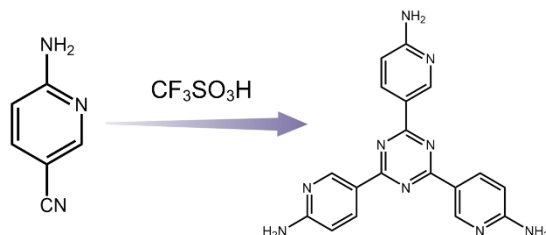


Figure-S4: Synthesis scheme of 5,5',5''-(1,3,5-triazine-2,4,6-triyl)tris(pyridin-2-amine).

S2.5. Synthesis of COF-A: COF-A was synthesized by following a previously reported procedure.^[1] 2-hydroxybenzene-1,3,5-tricarbaldehyde (14.3 mg, 0.08 mmol), 1,3,5-tris(4-aminophenyl)benzene (28.1 mg, 0.08 mmol), 0.5 mL of n-butanol, 0.5 mL of o-dichlorobenzene and 0.1 mL of 6 M aqueous acetic acid were added into a 20 mL glass vial. This mixture was sonicated for 15 mins. in order to get a homogenous dispersion. Then the tube was flash frozen at 77 K (liquid N_2 bath) and degassed. Thereafter, the tube was sealed and heated at $120\text{ }^{\circ}\text{C}$ for 7 days. A dark red colored precipitate produced was collected by filtration. Then it was washed and solvent exchanged with anhydrous tetrahydrofuran several times. The resultant precipitate was dried at $120\text{ }^{\circ}\text{C}$ under vacuum for overnight to give a red colored powder.

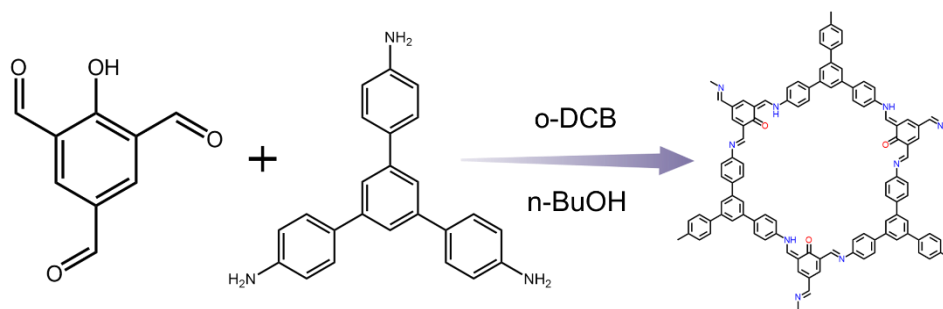


Figure-S5: Synthesis scheme of COF-A.

S2.6. Synthesis of COF-B: COF-B was synthesized by following a previously reported procedure with slight modification.^[5] 70.5 mg of 4,4',4''-(pyridine-2,4,6-triyl)trianiline (0.2 mmol) and 36 mg of 2-hydroxybenzene-1,3,5-tricarbaldehyde (0.2 mmol) were added in a 20 mL glass tube and dissolved in 2.5 ml o-dichlorobenzene and 2.5 ml n-butanol mixture. After that 0.5 ml of 6M acetic acid was added to this mixture and was stirred well. Then the tube was flash frozen at 77 K (liquid N₂ bath), degassed, and sealed. The contents in the sealed tube was heated at 120 °C for 3 days. After cooling to room temperature, the deep brown precipitate was filtered and washed with DMF, THF, MeOH. The powder was dried at 120°C, overnight. The final product was cleaned through soxhlet extraction.

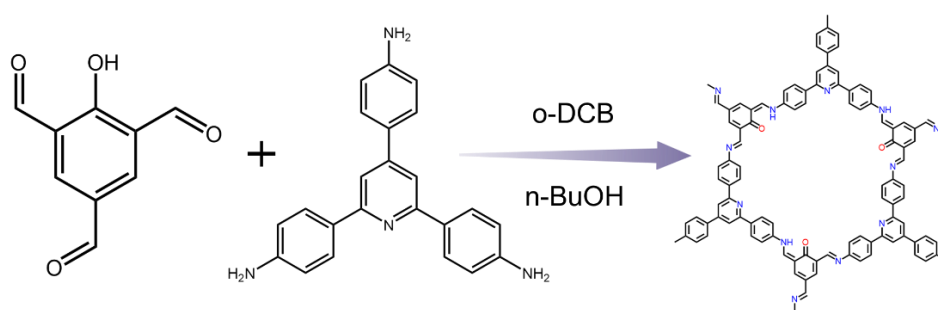


Figure-S6: Synthesis scheme of COF-B.

S2.7. Synthesis of COF-C: COF-C was synthesized by following a previously reported procedure with slight modification.^[6] In a typical synthetic procedure a 20 mL of pyrex tube was charged with 26.72 mg (0.15 mmol) of 2-hydroxybenzene-1,3,5-tricarbaldehyde (TFP) and 53.17 mg (0.15 mmol) of 2,4,6-tris(4-aminophenyl)-1,3,5-triamine (TAPT). Then 2.5 mL of mesitylene and 2.5 mL of dioxane along with 0.5 mL of 6M acetic acid were added to the mixture. After that, the tube was sonicated for 15 minutes in order to get a homogenous dispersion. Then the tube was flash frozen at 77 K (liquid N₂ bath) and degassed. Thereafter, the tube was sealed and heated at 120 °C for 3 days. After 3 days the sealed tube was taken out to obtain deep red-color material. Finally, it was collected and washed with dry solvents (methanol, acetone and THF) and dried at 120 °C for 6 hours.

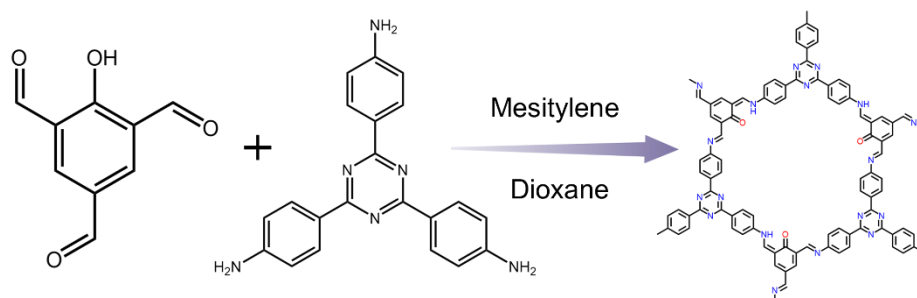


Figure-S7: Synthesis scheme of COF-C.

S2.8. Synthesis of COF-D: COF-D was synthesized by following a previously reported procedure with slight modification.^[4] 2-hydroxybenzene-1,3,5-tricarbaldehyde (53.5 mg, 0.3 mmol) and 5,5',5''-(1,3,5-triazine-2,4,6-triyl)tris(pyridin-2-amine) (107 mg, 0.3 mmol) were weighed into a Pyrex tube and were dissolved in 3 mL of dioxane and 3 mL of mesitylene and stirred until a red color was observed. To this mixture, 1.0 mL of stock acetic acid was added. Then the Pyrex tube was flash frozen in a liquid nitrogen bath and sealed. The Pyrex tube along with its contents was placed in an oven for heating at 120 °C for 5 days and gradually cooled to room temperature overnight. After cooling to room temperature, the dark-red colored precipitate was filtered and washed with DMF, THF, MeOH and THF. The final product was cleaned through soxhlet extraction and dried at 80 °C for 12 h.

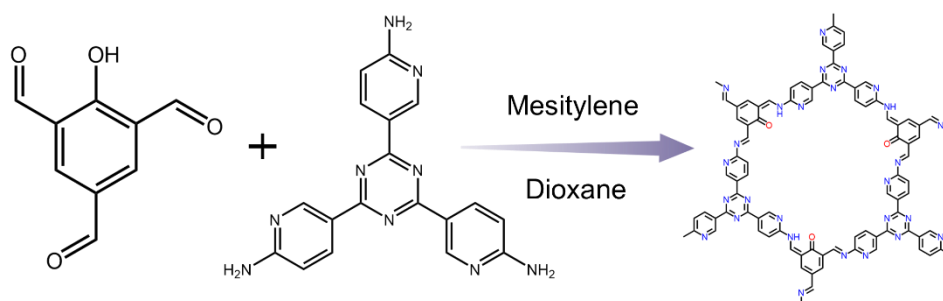


Figure-S8: Synthesis scheme of COF-D.

S2.9. Synthesis of COF-A1: The synthesis procedure of COF-A1 is almost similar to COF-A, however the precursor amount, solvent and catalyst was changed as following. 2-hydroxybenzene-1,3,5-tricarbaldehyde (26.8 mg, 0.15 mmol), 1,3,5-tris(4-aminophenyl)benzene (52.7 mg, 0.15 mmol), 2.5 mL of mesitylene, 2.5 mL of dioxan and 0.5 mL of 6 M aqueous acetic acid were added

into a 20 mL glass vial. This mixture was sonicated for 15 mins. in order to get a homogenous dispersion. Then the tube was flash frozen at 77 K (liquid N₂ bath) and degassed. Thereafter, the tube was sealed and heated at 120 °C for 3 days. Rest of the procedure is same as COF-A.

S2.10. Synthesis of COF-A2: The synthesis procedure of COF-A2 is almost similar to COF-A, however the precursor amount, solvent and catalyst was changed as following. 2-hydroxybenzene-1,3,5-tricarbaldehyde (26.8 mg, 0.15 mmol), 1,3,5-tris(4-aminophenyl)benzene (52.9 mg, 0.15 mmol), 2.5 mL of mesitylene, 2.5 mL of dioxan and 1 mL of 6 M aqueous acetic acid were added into a 20 mL glass vial. This mixture was sonicated for 15 mins. in order to get a homogenous dispersion. Then the tube was flash frozen at 77 K (liquid N₂ bath) and degassed. Thereafter, the tube was sealed and heated at 120 °C for 3 days. Rest of the procedure is same as COF-A.

S2.11. Synthesis of COF-A3: The synthesis procedure of COF-A3 is similar to COF-A, however the precursor amount, solvent and catalyst was changed as following. 2-hydroxybenzene-1,3,5-tricarbaldehyde (53.5 mg, 0.3 mmol), 1,3,5-tris(4-aminophenyl)benzene (105.4 mg, 0.3 mmol), 3 mL of mesitylene, 3 mL of dioxan and 0.5 mL of stock acetic acid were added into a 20 mL glass vial. This mixture was sonicated for 15 mins. in order to get a homogenous dispersion. Then the tube was flash frozen at 77 K (liquid N₂ bath) and degassed. Thereafter, the tube was sealed and heated at 120 °C for 3 days. Rest of the procedure is same as COF-A.

S2.12. Synthesis of COF-D1: The synthesis procedure of COF-D1 is similar to COF-D, however the precursor amount, solvent and catalyst was changed as following. 2-hydroxybenzene-1,3,5-tricarbaldehyde (53.5 mg, 0.3 mmol), 5,5',5''-(1,3,5-triazine-2,4,6-triyl)tris(pyridin-2-amine (107mg, 0.3 mmol), 2.5 mL of mesitylene, 2.5 mL of dioxan and 1.5 mL of stock acetic acid were added into a 10 mL glass vial. This mixture was sonicated for 15 mins. in order to get a homogenous dispersion. Then the tube was flash frozen at 77 K (liquid N₂ bath) and degassed. Thereafter, the tube was sealed and heated at 120 °C for 3 days. Rest of the procedure is same as COF-D.

Section-S3: Experimental section

S3.1. General Consideration: The aqueous solution of organic dyes were prepared by dissolving a certain amount of solid dye into deionized water and the different concentrations were obtained by diluting the stock solution with the proper amount of distilled water unless otherwise indicated. The concentrations of dyes during all the experiments were detected by UV-vis spectroscopic analysis. All the adsorption experiments were performed at ambient conditions. All the data has been collected three times through UV-vis analysis to plot the final adsorption results.

S3.2. Vapor phase static organic iodide uptake studies: Typically, ~15 mg of desolvated COF sample was weighted in a small glass vial, and this vial was exposed to organic iodide (CH_3I or $\text{C}_2\text{H}_5\text{I}$) (~3 mL) at 75 °C (348 K) in a closed system. After the corresponding adsorption time, the glass vial was taken out, cooled to room temperature, and weighed. Organic iodide uptake capacity of the sample was calculated by the weight difference of glass vials before and after adsorption, using the formula:

$$w = \frac{(m_2 - m_1)}{m_1} \times 100\% \quad \dots\dots\dots(1)$$

Where, w (g.g^{-1}) is the adsorption capacity of organic iodide uptake, m_1 (g) and m_2 (g) are the mass of compounds with the glass vial before and after being exposed to organic iodide vapor. The values of uptake capacity are the average values of at least three experiments. In case of other temperatures, such as 273 and 423 K, similar static CH_3I adsorption experiment was conducted in a closed system.

S3.3. Recyclability test: To study the recyclability for CH_3I -loaded material in static system we followed a reported protocol with slight modification.^[7] Typically, a certain amount of CH_3I -loaded compound with maximum adsorption capacity was taken in an glass vial containing excess amount of ethanol and ultrasonicated for a certain period of time. Thereafter, the regenerated samples were dried under vacuum at 120 °C overnight and then reused for the next cycle CH_3I adsorption test in static phase.

S3.4. Retention ability test: To study the adsorption stability for methyl iodide-loaded material in static system, a certain amount of CH_3I -loaded material was taken in an open glass vial, and the vial was placed in an empty large bottle, which was placed open at room temperature and ambient pressure. After one day, the weight of the vial containing CH_3I -adsorbed material was recorded and the vial was placed

back into the empty large bottle. The large bottle was opened to further continue the experiment for next 7 days.

S3.5. Vapor phase dynamic methyl iodide uptake studies: The gaseous methyl iodide adsorption in dynamic system was performed in a home-built setup. At first, 20 mg of COF sample was packed into a glass column with glass wool filling the void space of both ends, which served as the adsorption cell. This adsorption cell along with a separate chamber containing methyl iodide was transferred into an oven and heated at 75 °C for desired time period. A nitrogen flow (5 cm³/min) passed through the methyl iodide vapor generator (inlet) to blow the methyl iodide vapor into the COF material in the adsorption cell. The effluent from the adsorption cell (outlet) was treated with 0.1 M NaOH solution. The adsorption capacity for methyl iodide was calculated from the weight difference of glass tubes before and after adsorption. The vapor phase dynamic methyl iodide capture study in the presence of nitric acid vapor was performed in a similar method taking HNO₃ in a separate glass vial along with the methyl iodide vial (Figure-4 in main text).

S3.6. Organic dyes capture experiments: The pollutant concentration was calculated by using UV-vis spectroscopy after establishing a standard curve at room temperature. The pollutant removal efficiency (%) by the adsorbent polymer under investigation was determined utilizing the following equation:

$$\text{Removal efficiency} = \frac{(C_0 - C_t)}{C_0} \times 100\%$$

Where, C₀ (mM) and C_t (mM) represents the concentrations of pollutant solutions before and after adsorption, respectively.

The amount of pollutant adsorbed by the polymer was calculated from the following equation:

$$\text{Adsorption capacity (qt)} = \frac{(C_0 - C_t)}{m} \times \text{Mw}$$

Where, qt (mg.g⁻¹) is the amount of pollutant adsorbed per gm of adsorbent material at time t (min). C₀ (mmol.L⁻¹) and C_t (mmol.L⁻¹) represent the initial and residual concentration of pollutant in the stock solution and filtrate, respectively; m (gm) is the mass of adsorbent used for the study. Mw (g.mol⁻¹) is the molar mass of the dyes under consideration.

S3.7. Organic dyes adsorption kinetics study: Initially 2 mL 0.1 mM aqueous stock solution of the respective organic dyes were taken in a UV cuvette and subsequently their initial absorbance was

measured. 2 mg of COFs was added to the dye solution and the absorbance spectra of the supernatant solutions were recorded accordingly at different time intervals. The concentration of the dyes in the filtrate was determined by UV-Vis spectroscopy subsequently.

The adsorption kinetics were further quantified utilizing pseudo-second-order model from which the apparent rate constant k_{obs} can be obtained using following equation:

$$t/q_t = t/q_e + 1/k_{obs}q_e^2$$

Where, q_t and q_e are the adsorbate uptakes (mg adsorbate per gm of COFs) at time t (min) and at equilibrium, respectively, and k_{obs} is an apparent second-order rate constant ($\text{g}\cdot\text{mg}^{-1}\cdot\text{min}^{-1}$). The rate constant k_{obs} can be calculated from the intercept and slope of the plot of t/q_t against t .

S3.8. Column-exchange based dye capture experiment: To check the dye removal efficiency of COF-A after CH_3I adsorption ($\text{CH}_3\text{I}@$ COF-A), a column exchange-based sorption experiment was conducted by packing ~100 mg of $\text{CH}_3\text{I}@$ COF-A with ~5 gm of sand inside a U shaped glass column as bed for orange G (OG) as a model dye capture test (Figure-S71). Then different volume of stock 0.25 mmol OG aqueous solution was passed through the column bed with a flow rate of 0.5 mL/min, which was controlled by a water-flow-regulator, and the drops per minute was recorded with the help of a stopwatch. A bed-volume of ~2.1 mL of column eluted solution was collected in different containers. The concentration of the column eluted solutions were then analyzed through UV-vis spectroscopy (Figure-S72).

Section-S4: Theoretical calculation and simulation studies

Determination of electrostatic surface potential (ESP), binding sites and binding energy of different interactions:

Density functional theory (DFT) computations were performed using the Discovery Studio 2016 to derive the ESP surface of model monomers of COF-A, B, C and D. The geometry optimization of the monomers were carried out using hybrid B3LYP exchange correlation function and double numeric plus polarization (DNP) basis set with SCF density convergence of 1×10^{-6} . The electrostatic potential (ESP) on the van der Waals (VDW) surfaces (isodensity = 0.001 a.u.) of COF-A to COF-D monomers was derived based on its ground state electron density.

The Static binding energies (ΔE) at 0 K in vacuum were calculated using the following expression:

$$\Delta E = E(\text{COF} + \text{CH}_3\text{I}) - E(\text{COF}) - E(\text{CH}_3\text{I})$$

Where, E_x refers, respectively, to the total energies of the COF + CH₃I complex, the COF alone, and the CH₃I molecule respectively.

Section S5: Structural characterizations of the COFs

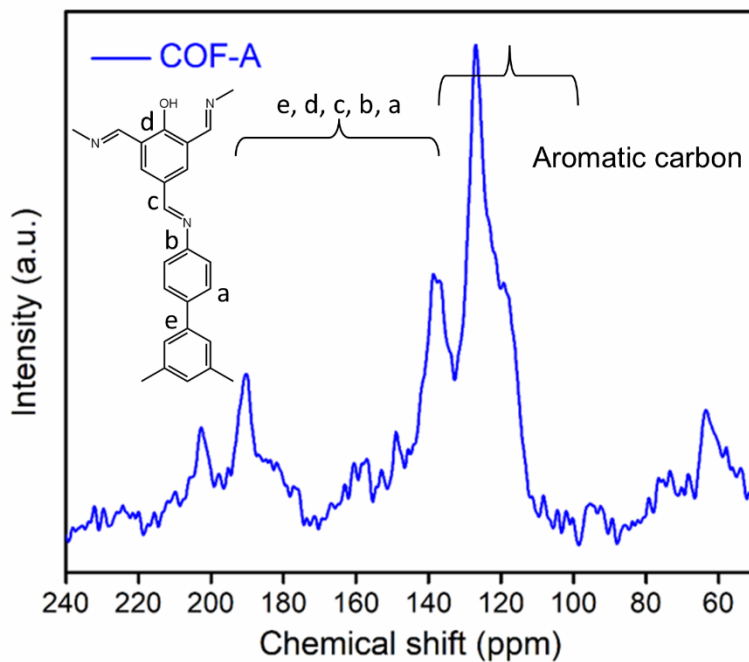


Figure-S9: Solid-state ^{13}C CP-MAS NMR spectra of COF-A.

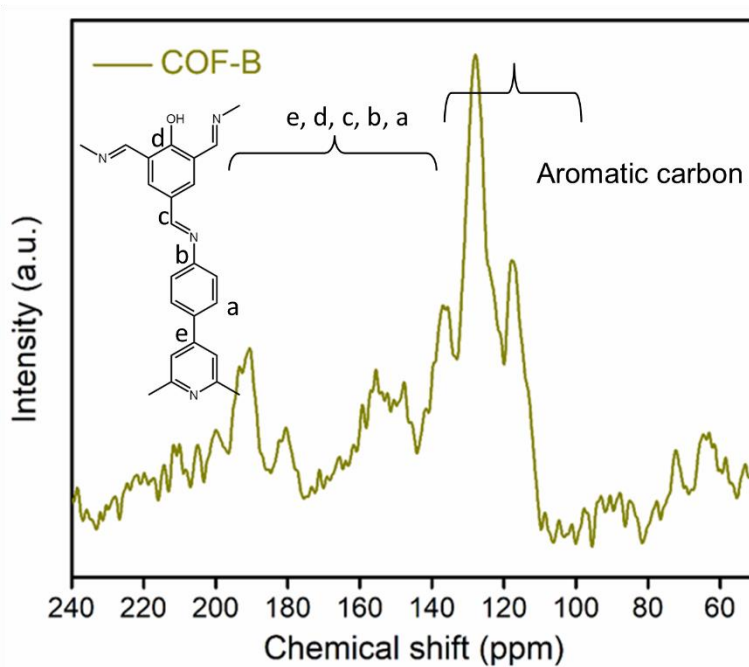


Figure-S10: Solid-state ^{13}C CP-MAS NMR spectra of COF-B.

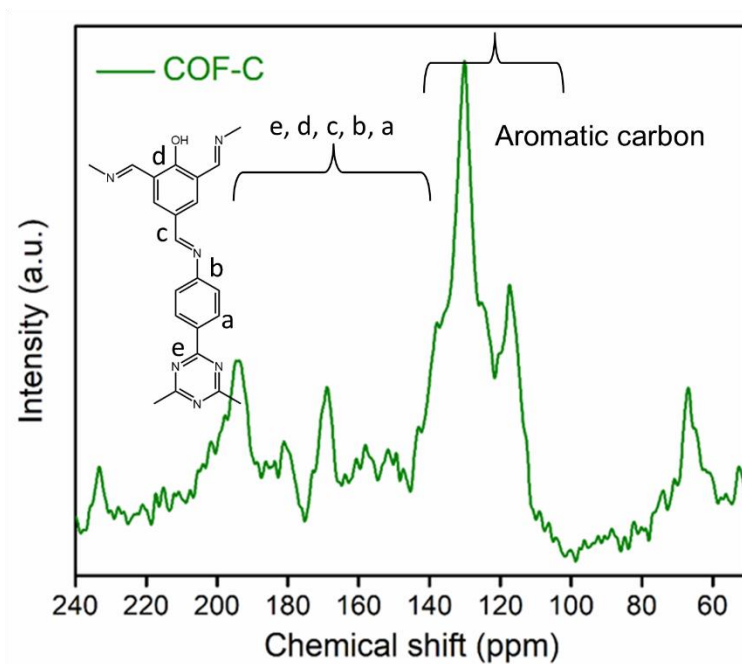


Figure-S11: Solid-state ^{13}C CP-MAS NMR spectra of COF-C.

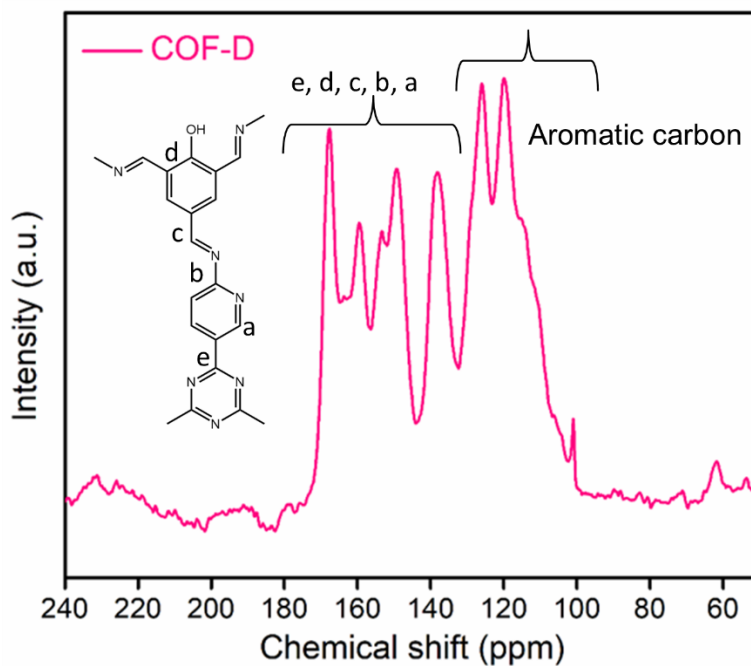


Figure-S12: Solid-state ^{13}C CP-MAS NMR spectra of COF-D.

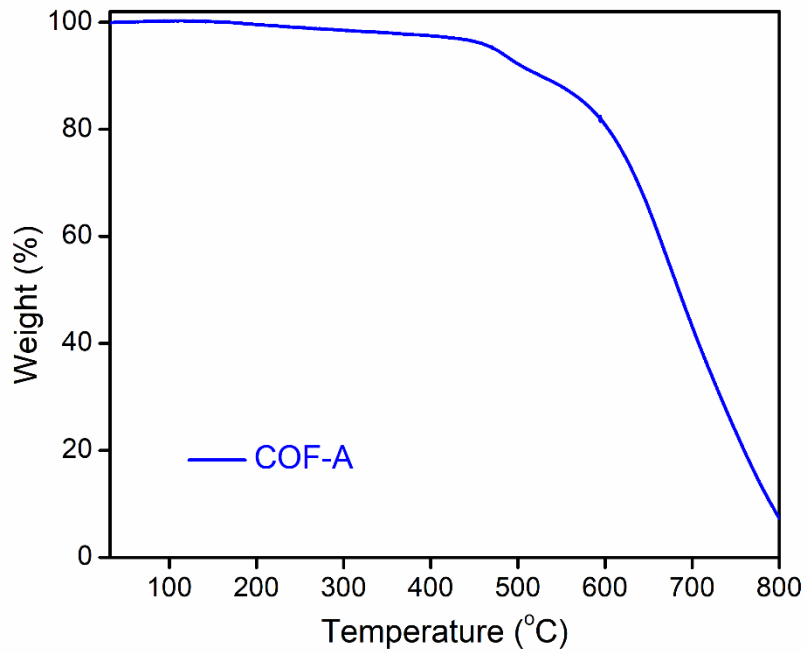


Figure-S13: TGA profile of COF-A.

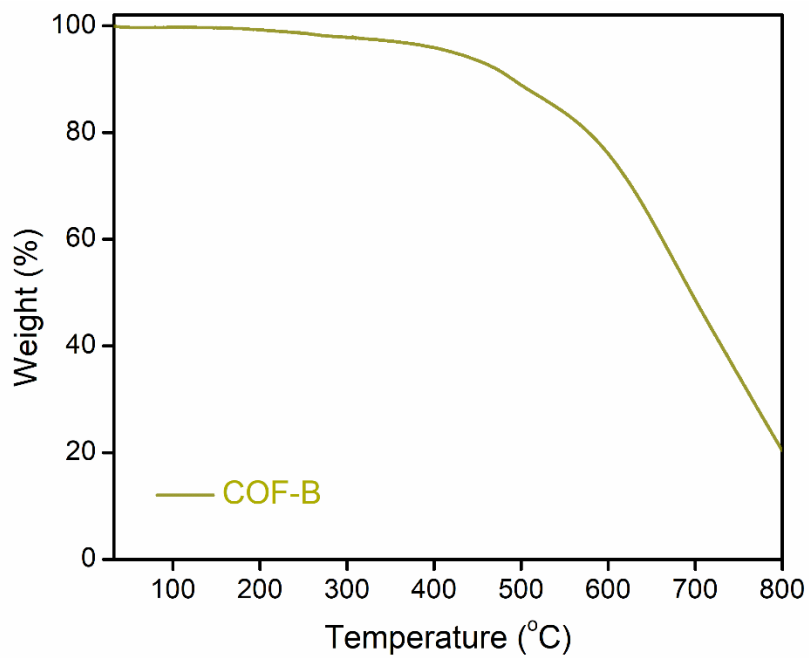


Figure-S14: TGA profile of COF-B.

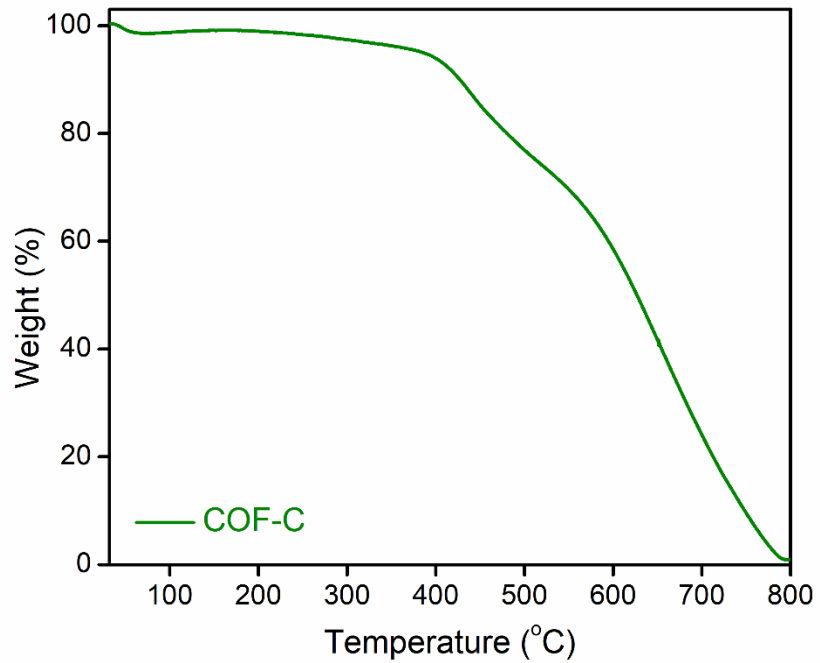


Figure-S15: TGA profile of COF-C.

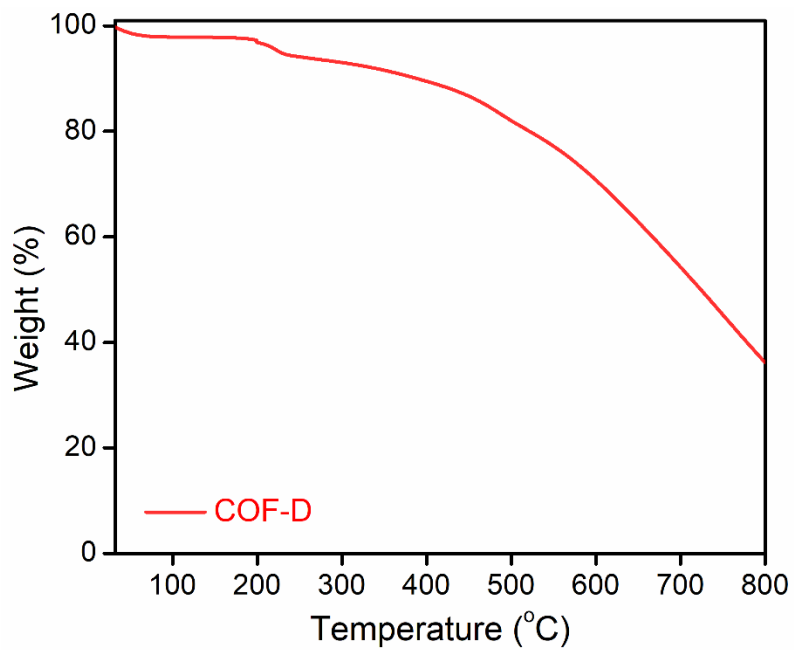


Figure-S16: TGA profile of COF-D.

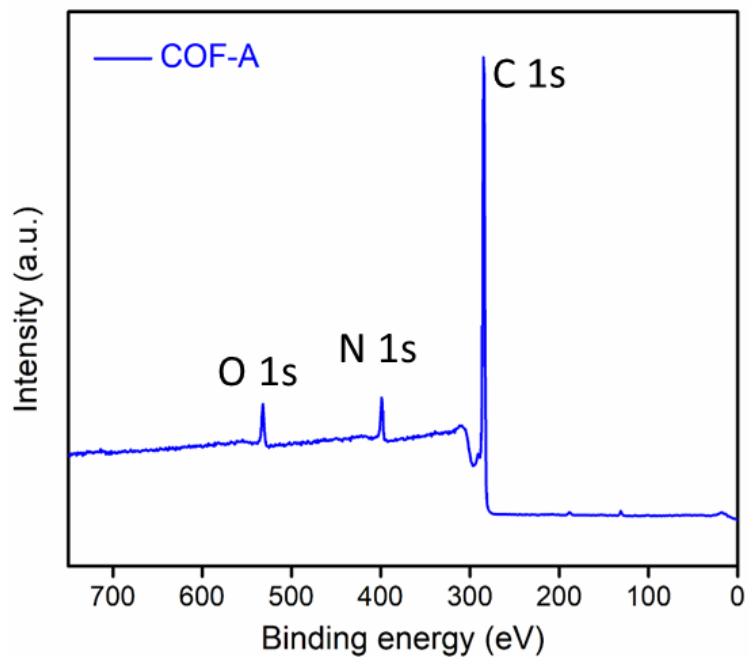


Figure-S17: XPS survey spectra of COF-A, showing the presence of C, N and O elements.

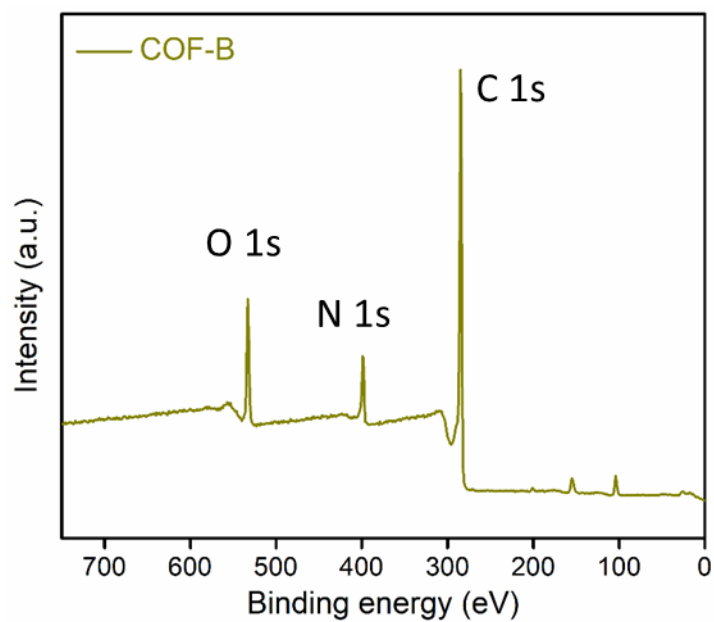


Figure-S18: XPS survey spectra of COF-B, showing the presence of C, N and O elements.

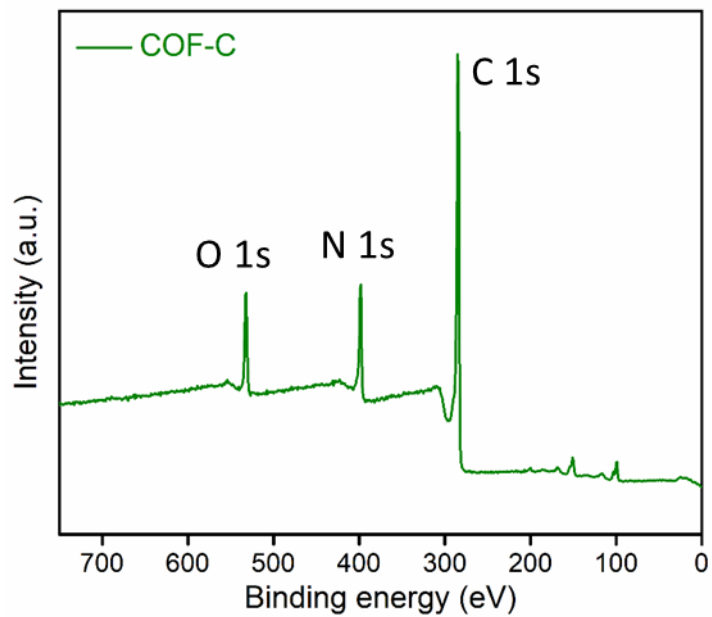


Figure-S19: XPS survey spectra of COF-C, showing the presence of C, N and O elements.

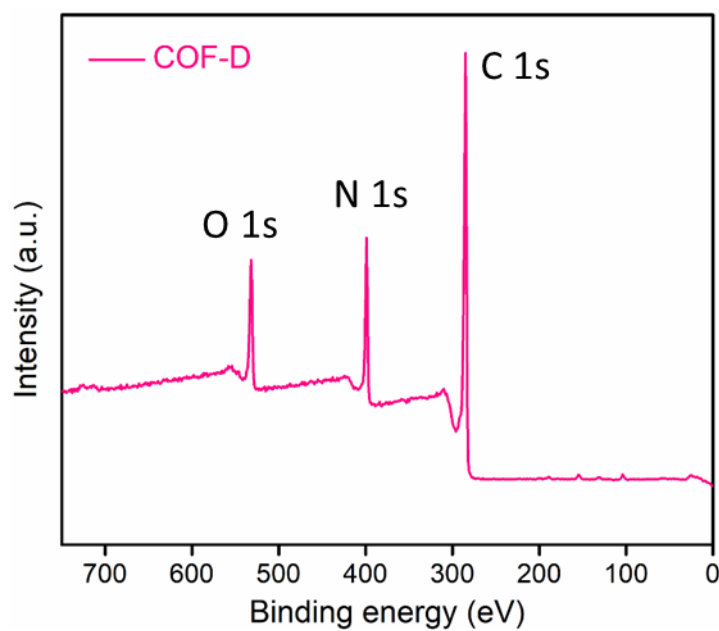


Figure-S20: XPS survey spectra of COF-D, showing the presence of C, N and O elements.

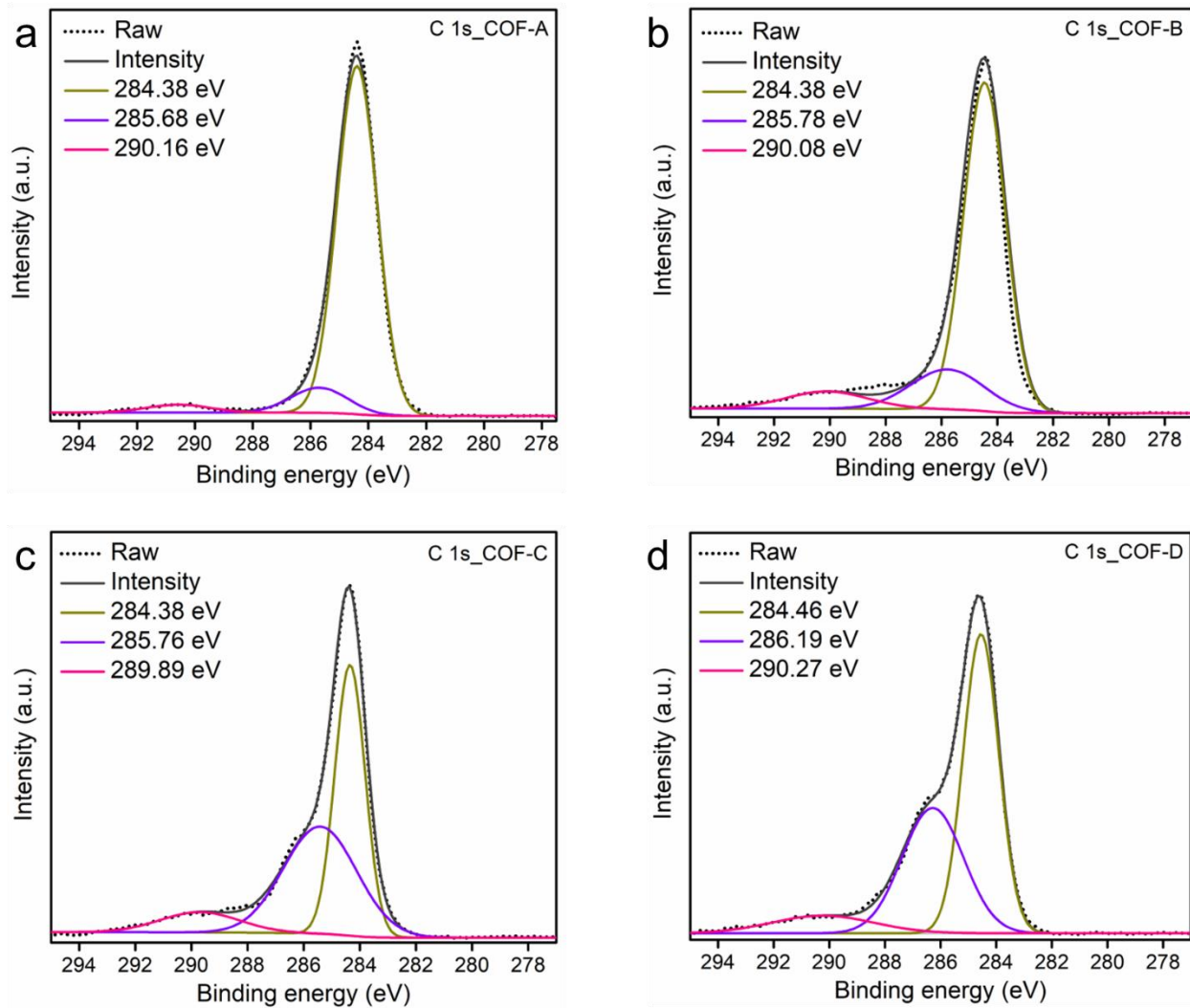


Figure-S21: C 1s XPS spectra of (a) COF-A, (b) COF-B, (c) COF-C, and (d) COF-D.

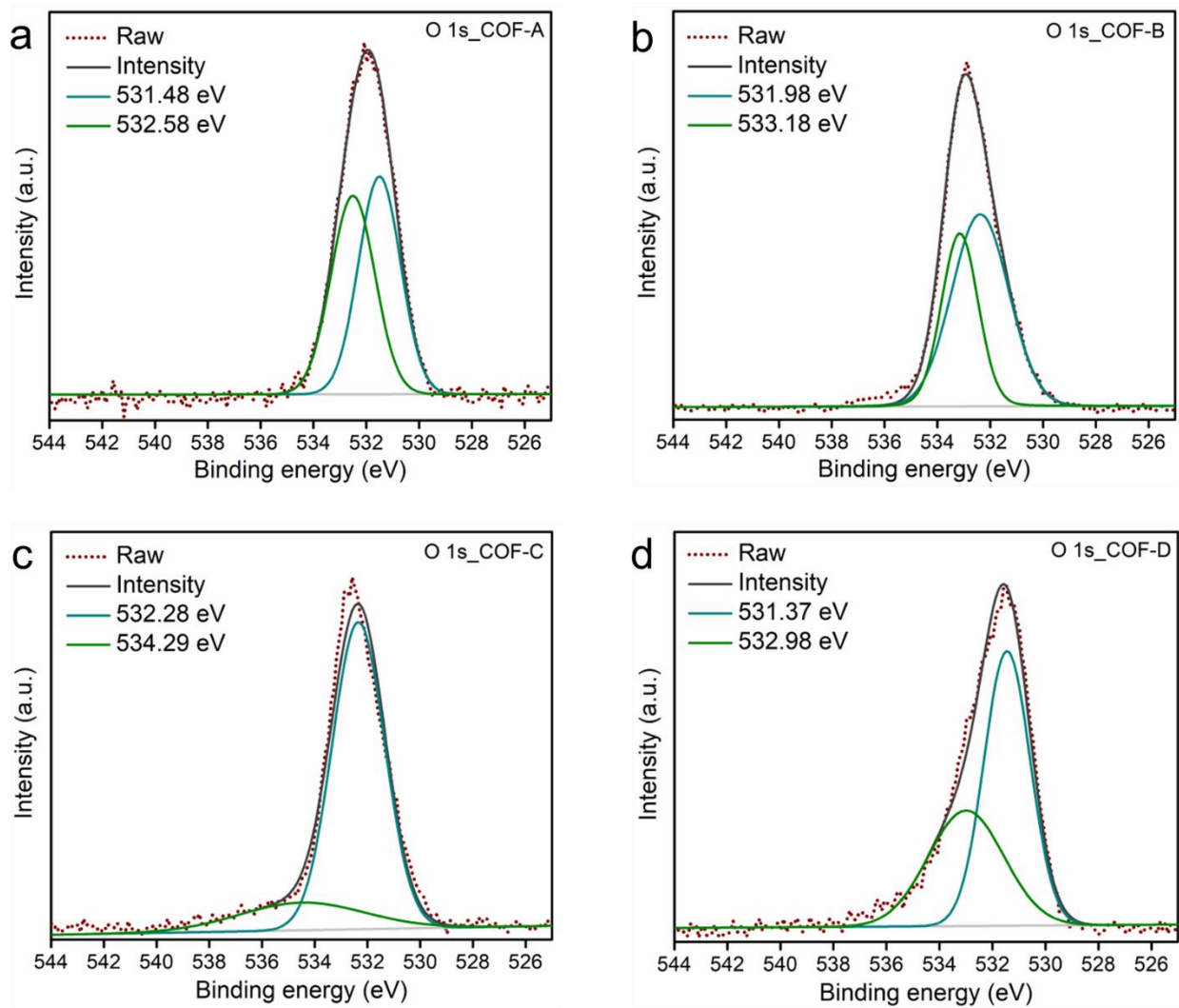


Figure-S22: O 1s XPS spectra of (a) COF-A, (b) COF-B, (c) COF-C, and (d) COF-D.

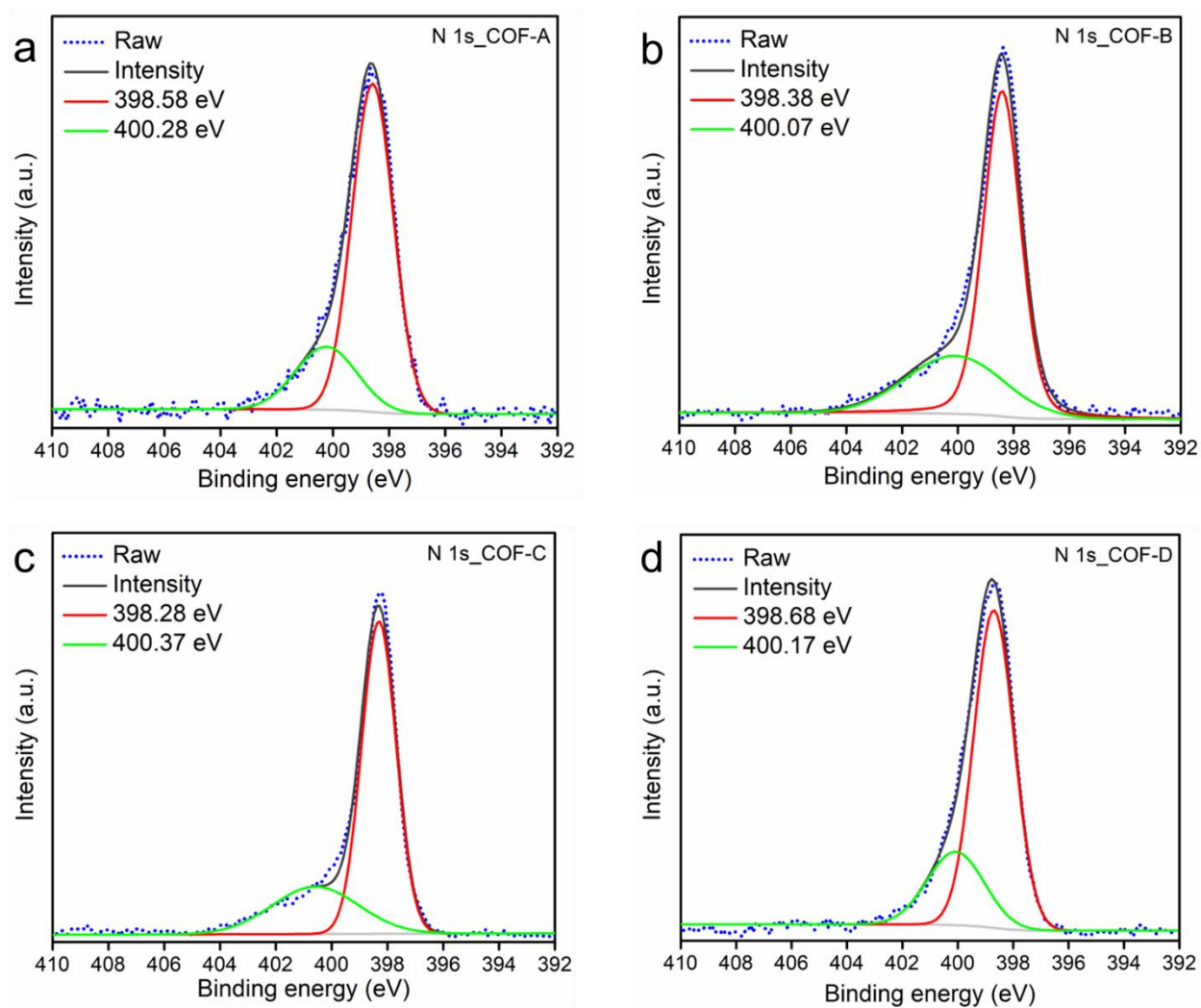


Figure-S23: N 1s XPS spectra of (a) COF-A, (b) COF-B, (c) COF-C, and (d) COF-D.

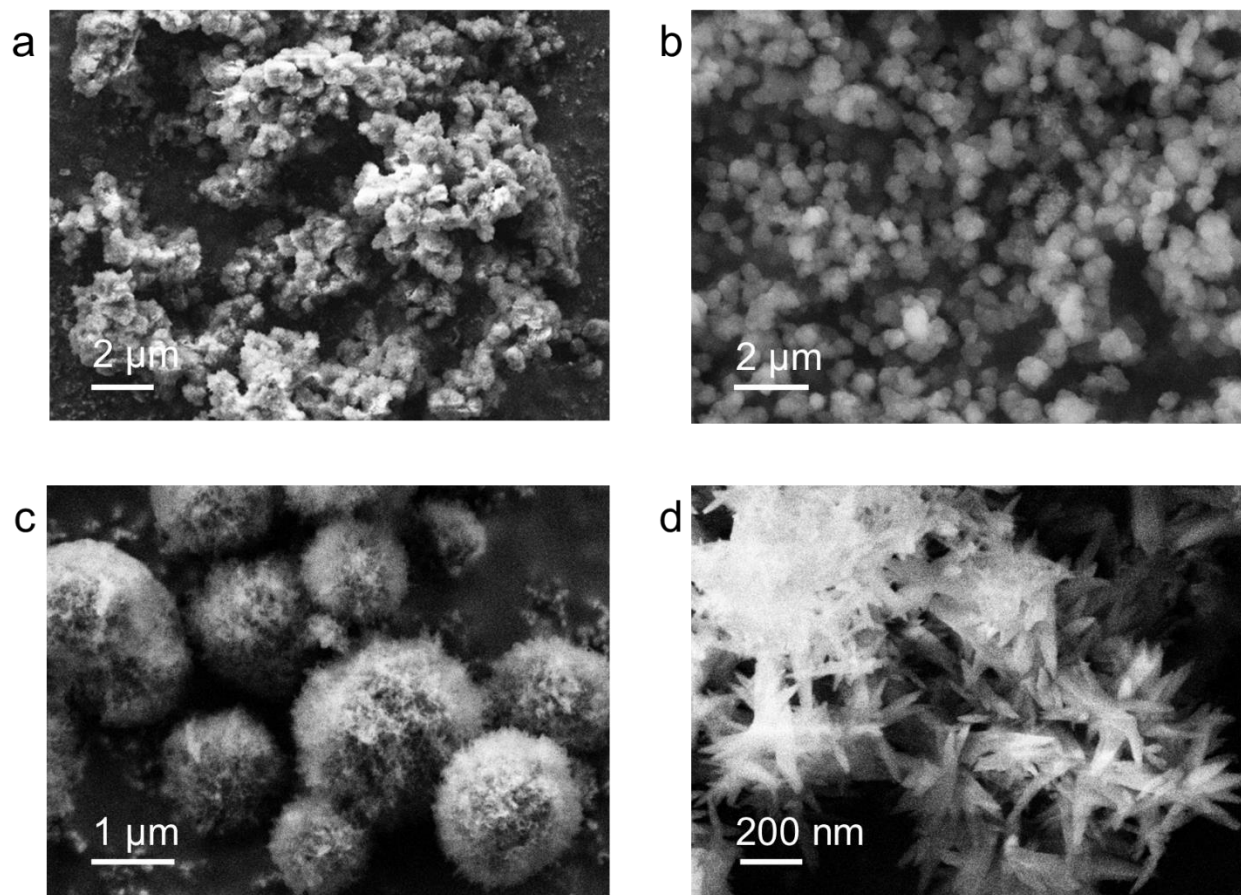


Figure-S24: FESEM images of (a) COF-A, (b) COF-B, (c) COF-C, and (d) COF-D.

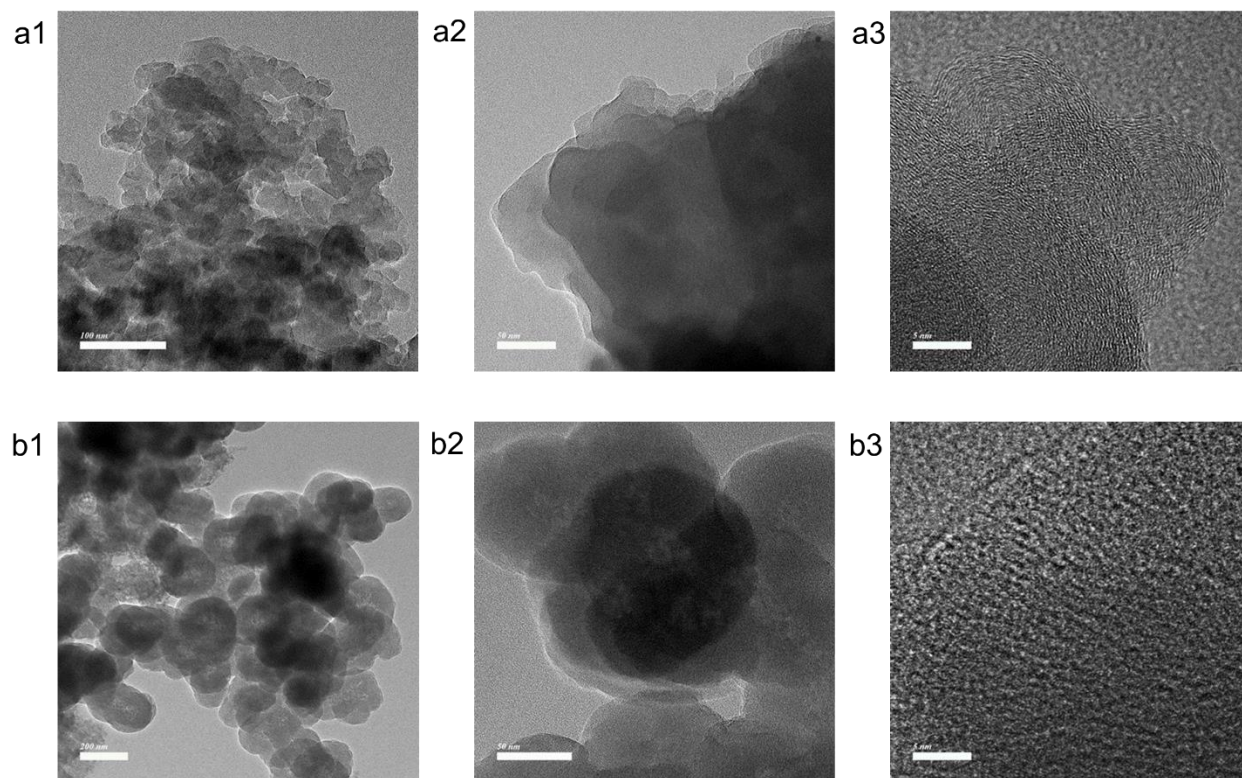


Figure-S25: TEM and HRTEM images of (a1-a3) COF-A and (b1-b3) COF-B.

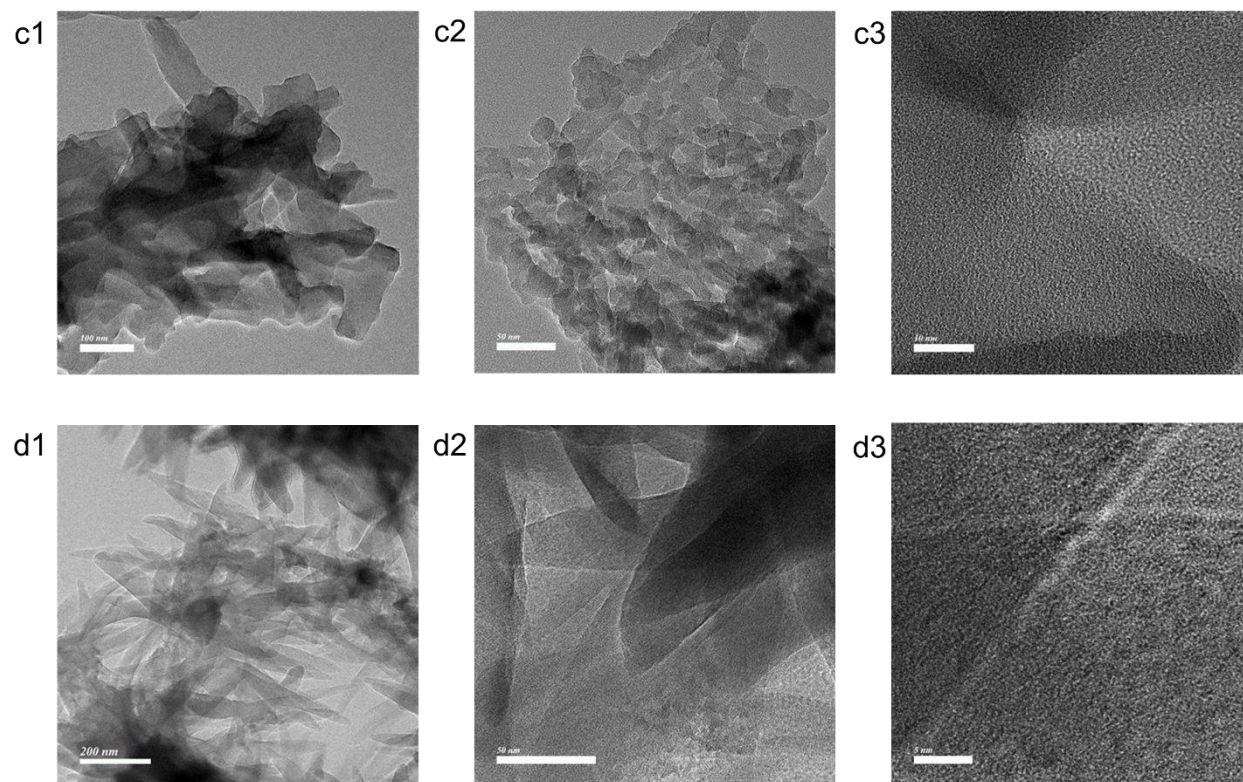


Figure-S26: TEM and HRTEM images of (c1-c3) COF-C and (d1-d3) COF-D.

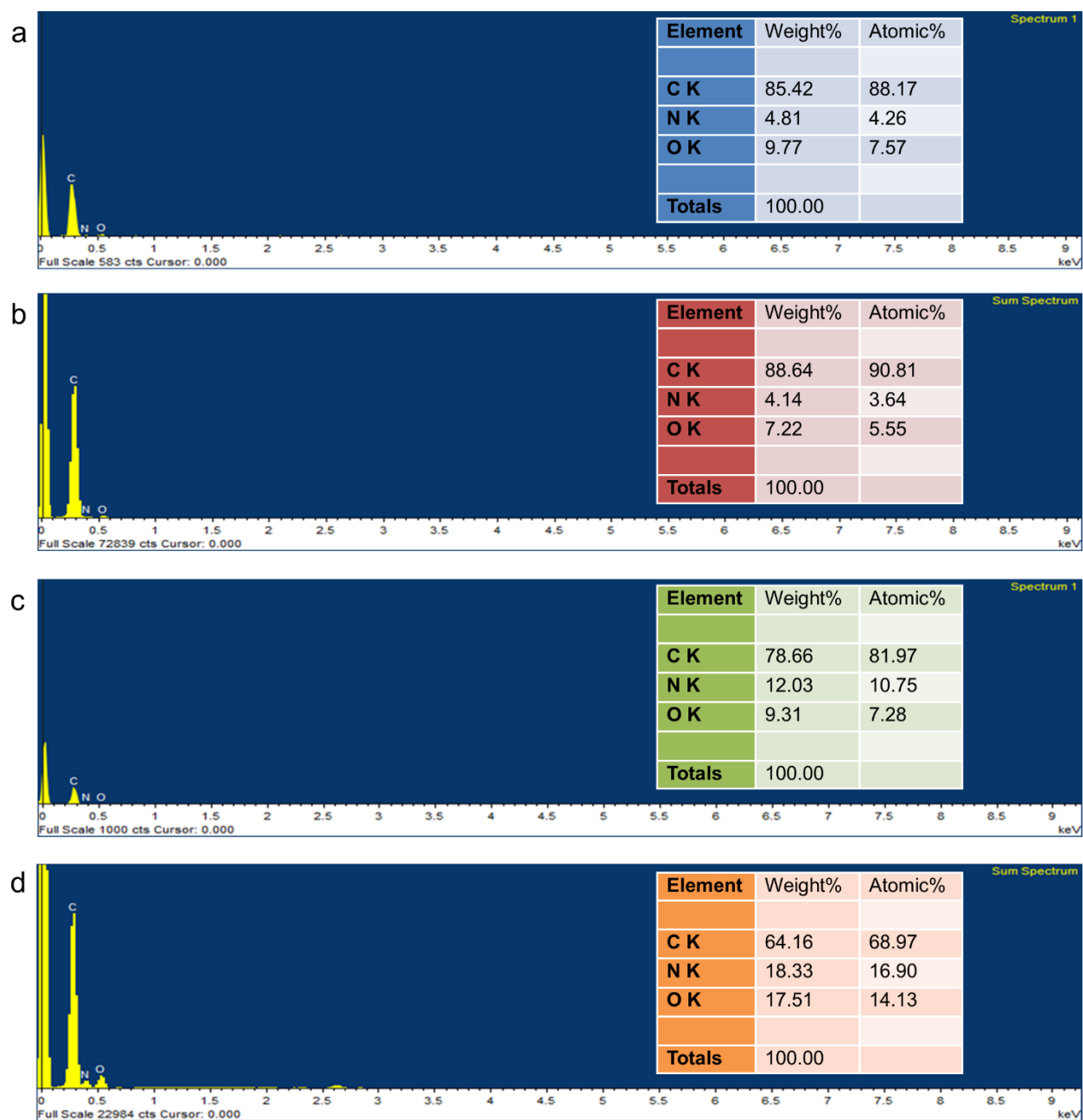


Figure-S27: Energy-dispersive X-ray spectroscopy (EDS) data from FESEM experiment of (a) COF-A, (b) COF-B, (c) COF-C, and (d) COF-D.

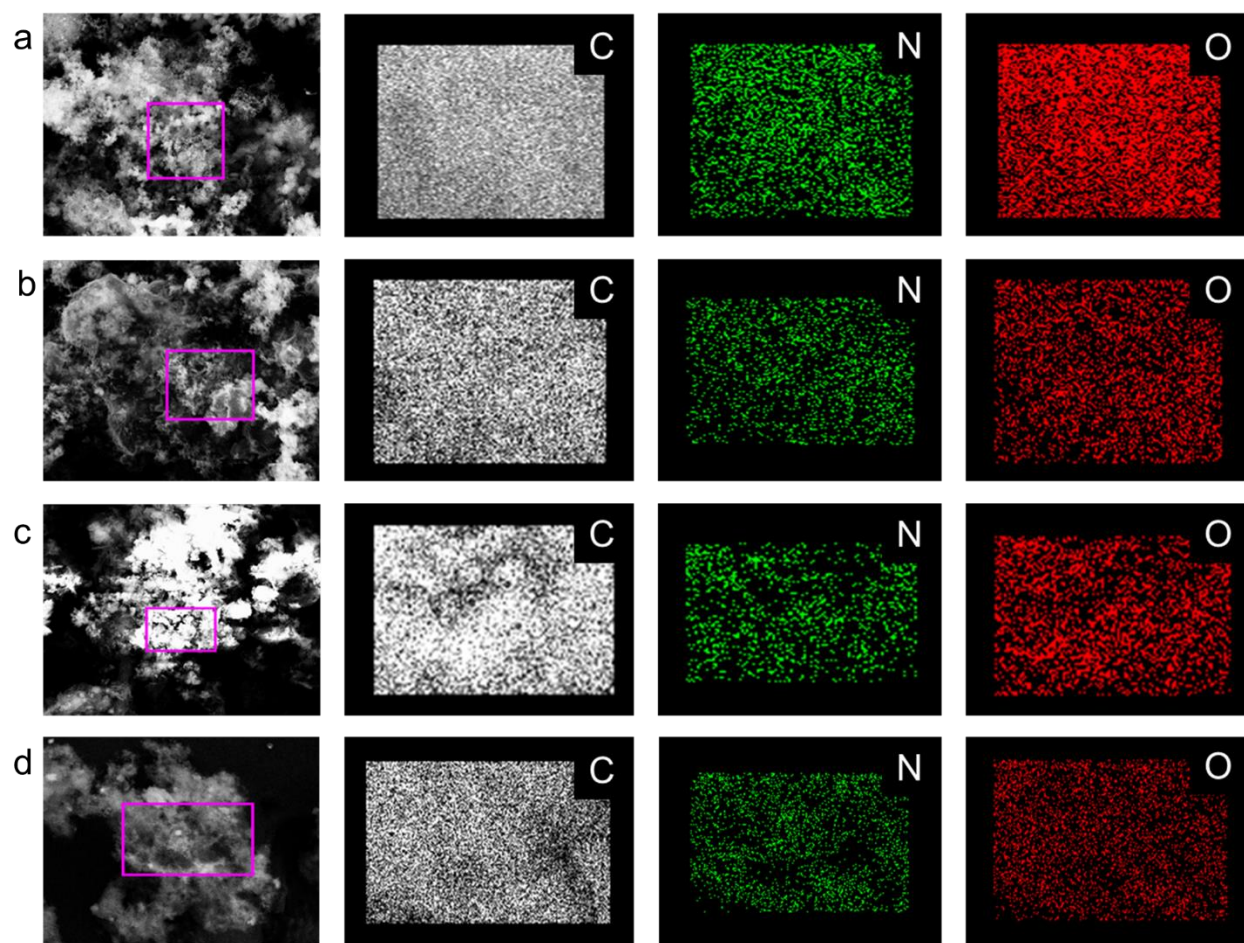


Figure-S28: Elemental mapping images from FESEM experiment of (a) COF-A, (b) COF-B, (c) COF-C, and (d) COF-D.

Table-S1: Elemental analysis data of the COF-A, COF-B, COF-C and COF-D.

Samples	Theoretical content			Experimental content		
	C [%]	H [%]	N [%]	C [%]	H [%]	N [%]
COF-A	78.89	6.14	14.97	79.88	3.95	16.17
COF-B	76.47	5.79	17.74	77.82	3.99	18.19
COF-C	72.96	6.27	20.77	74.05	4.10	21.85
COF-D	68.26	5.51	26.23	69.14	3.75	27.11

Section S6: Organic iodide capture study results.

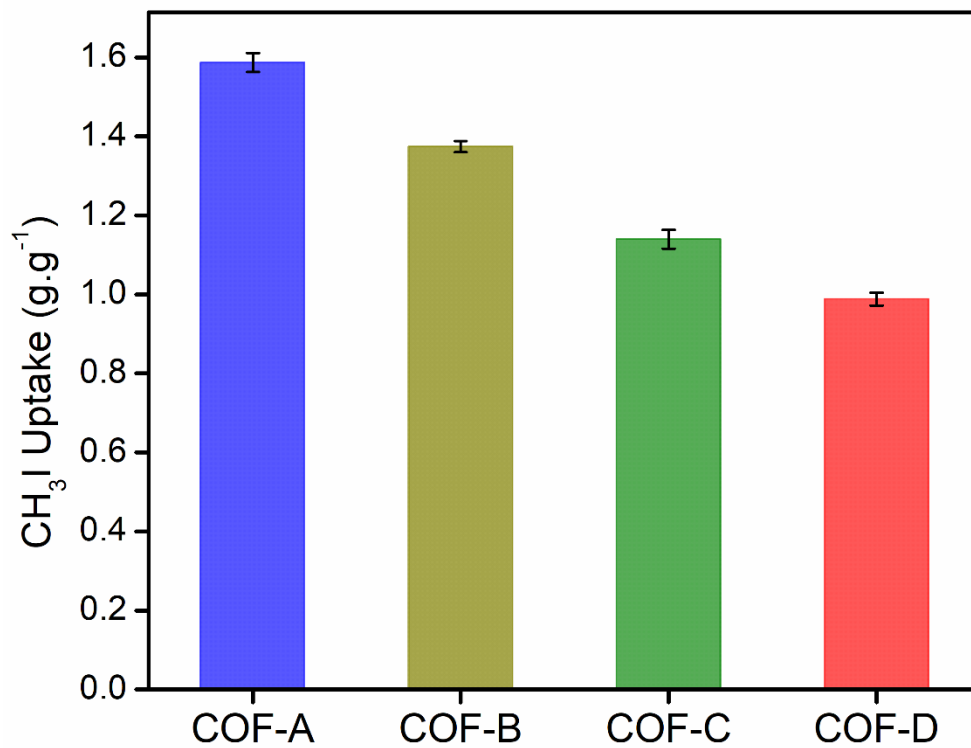


Figure-S29: Static CH_3I adsorption data of COF-A, COF-B, COF-C, and COF-D at 348 K.

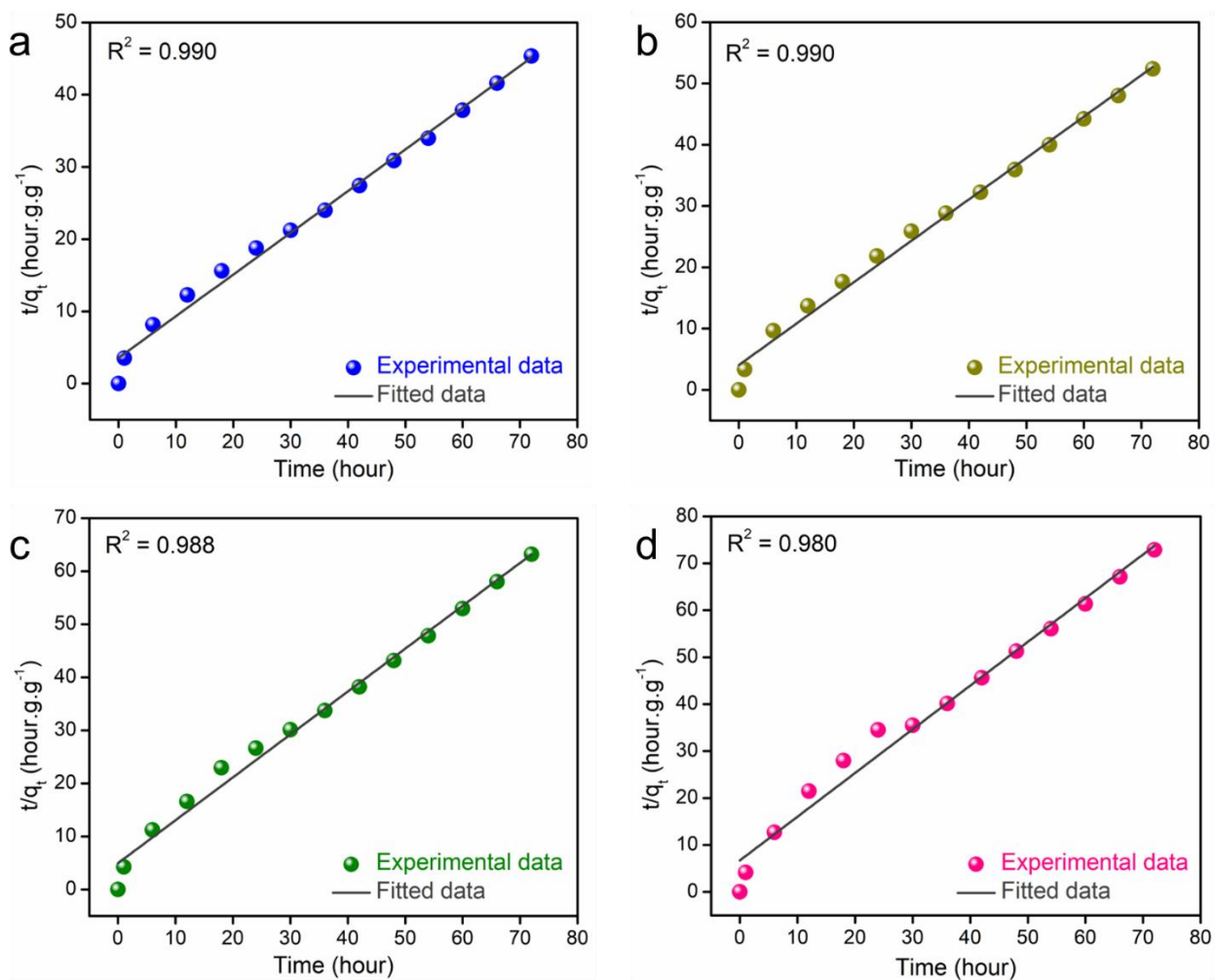
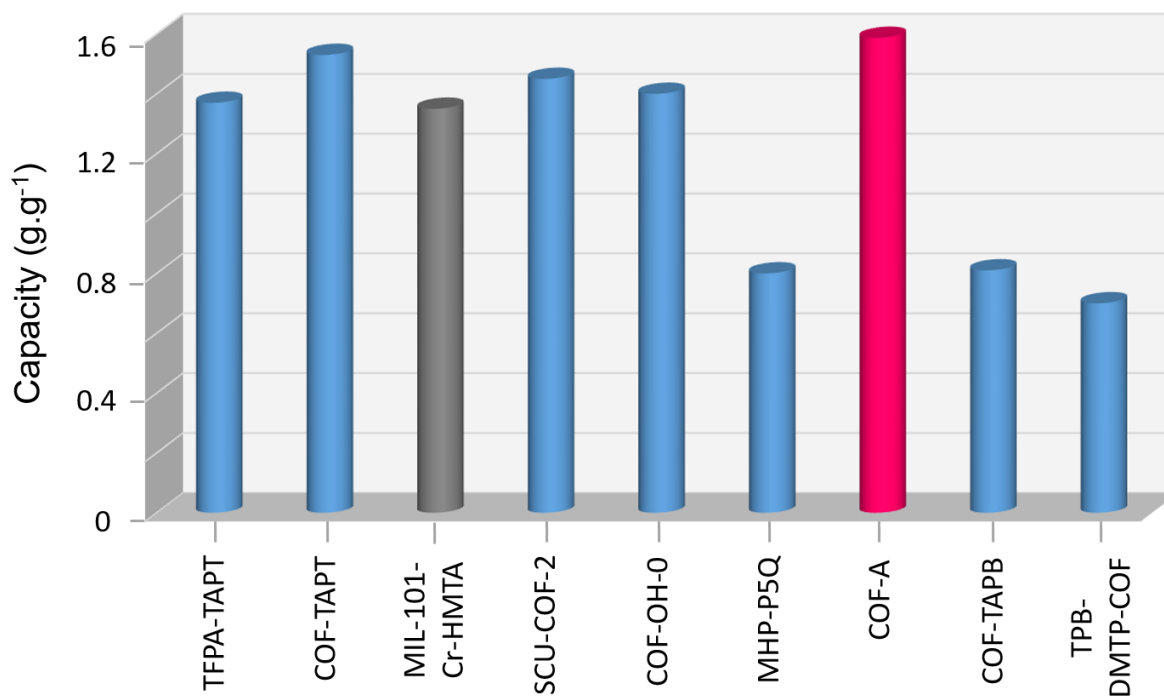


Figure-S30: Pseudo-second-order kinetic model fitting data of (a) COF-A, (b) COF-B, (c) COF-C, and (d) COF-D for CH_3I adsorption.

Table-S2: Comparison table of static CH₃I adsorption data of various reported adsorbents.

Sample	Temp.	CH ₃ I capacity	References
COF-A	348	1.58 g.g ⁻¹	This work
TFPA-TAPT	348	1.37 g.g ⁻¹	Nat. Commun. 2022, 13, 2878.
COF-TAPT	348	1.53 g.g ⁻¹	Nat. Commun. 2022, 13, 2878.
MIL-101-Cr-HMTA	348	1.35 g.g ⁻¹	Nat. Commun. 2017, 8, 485.
SCU-COF-2	348	1.45 g.g ⁻¹	Chem 2021, 7, 699–714.
COF-OH-0	348	1.4 g.g ⁻¹	Angew. Chem. Int. Ed. 2021, 60, 22432–22440.
MHP-P5Q	348	0.8 g.g ⁻¹	Nat. Commun. 2020, 11, 1086.
COF-TAPB	348	0.81 g.g ⁻¹	Nat. Commun. 2022, 13, 2878.
TPB-DMTP-COF	348	0.7 g.g ⁻¹	Adv. Mat. 2018, 30, 1801991.



Section S7: Chemical stability test and CH₃I adsorption study.

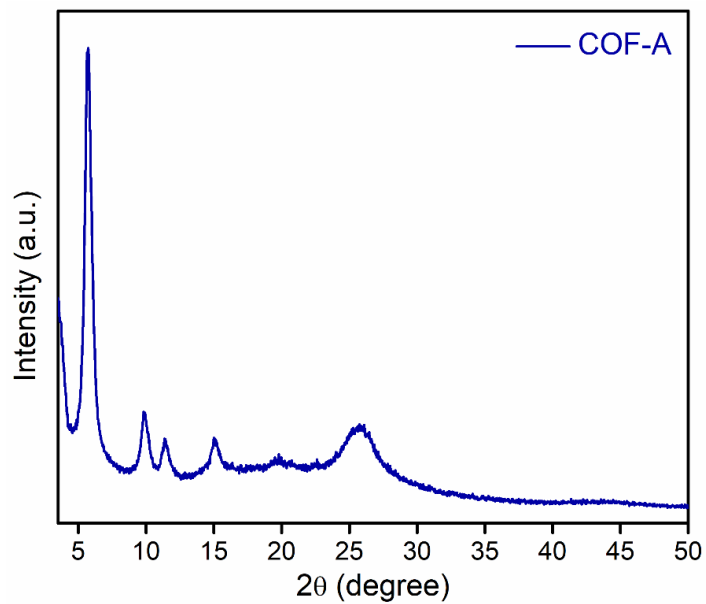


Figure-S31: PXRD profile of acid (1M HNO₃) treated COF-A.

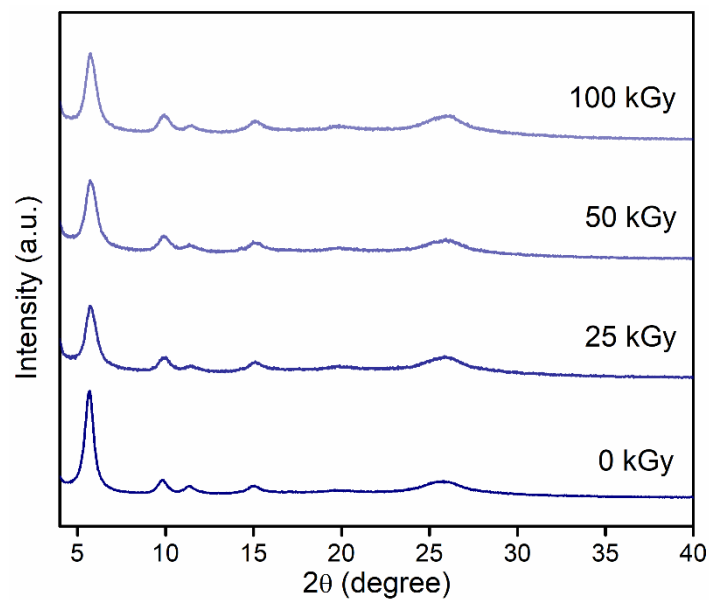


Figure-S32: PXRD profile of COF-A upon irradiation of different kGy radiation.

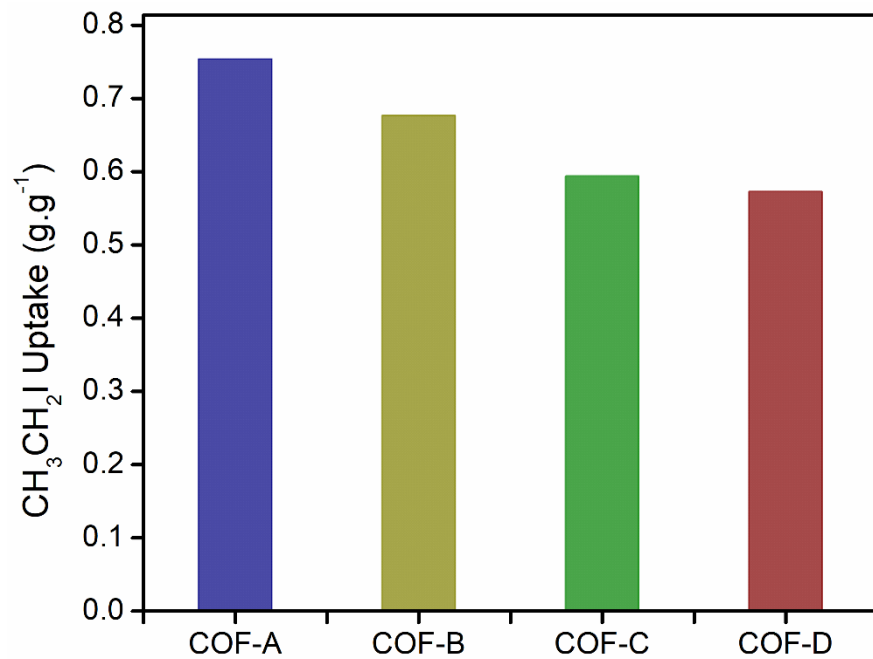


Figure-S33: Static adsorption capacities of CH₃CH₂I by COF-A at 348 K.

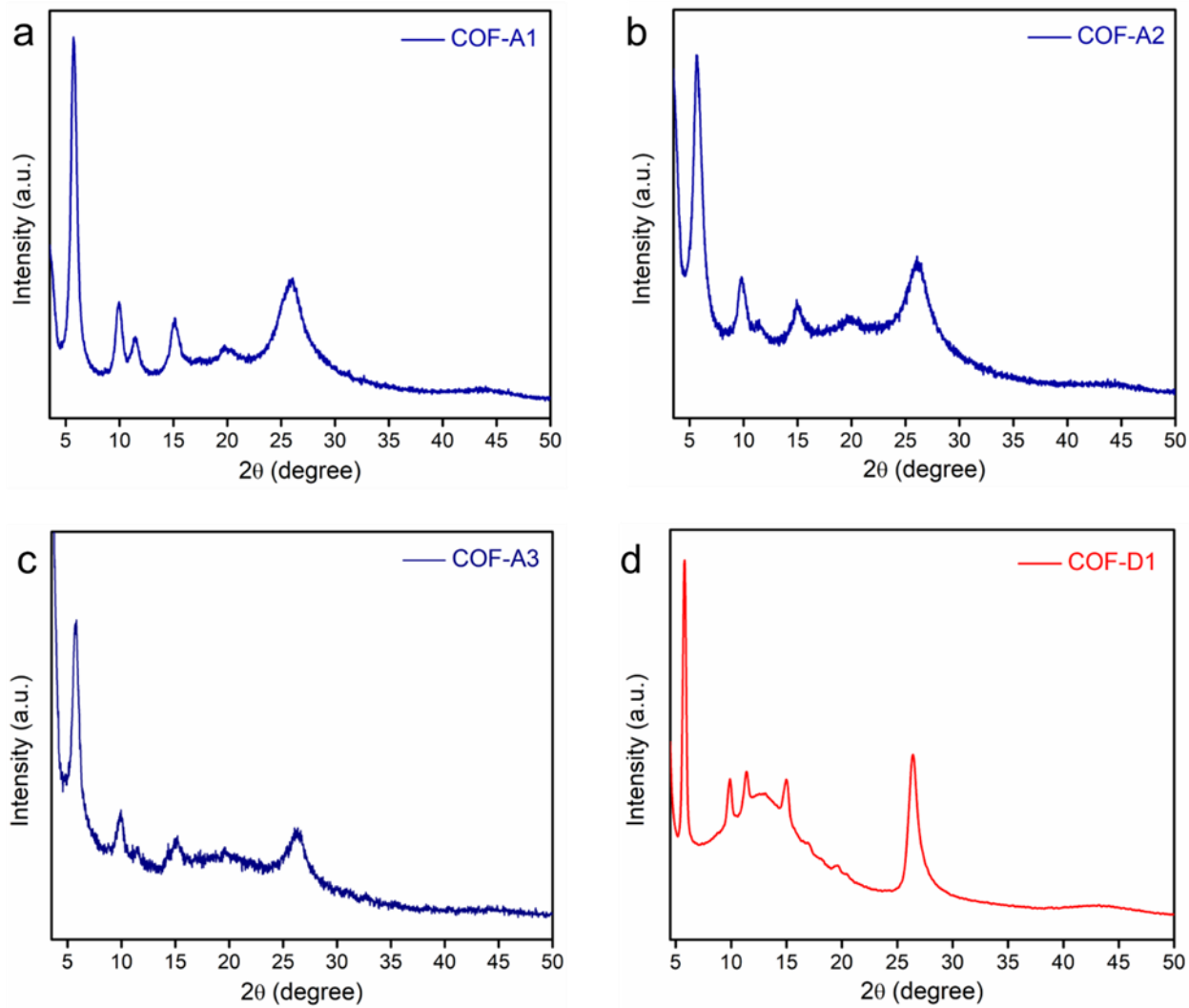


Figure-S34: PXR D patterns of (a) COF-A1, (b) COF-A2, (c) COF-A3, and (d) COF-D1.

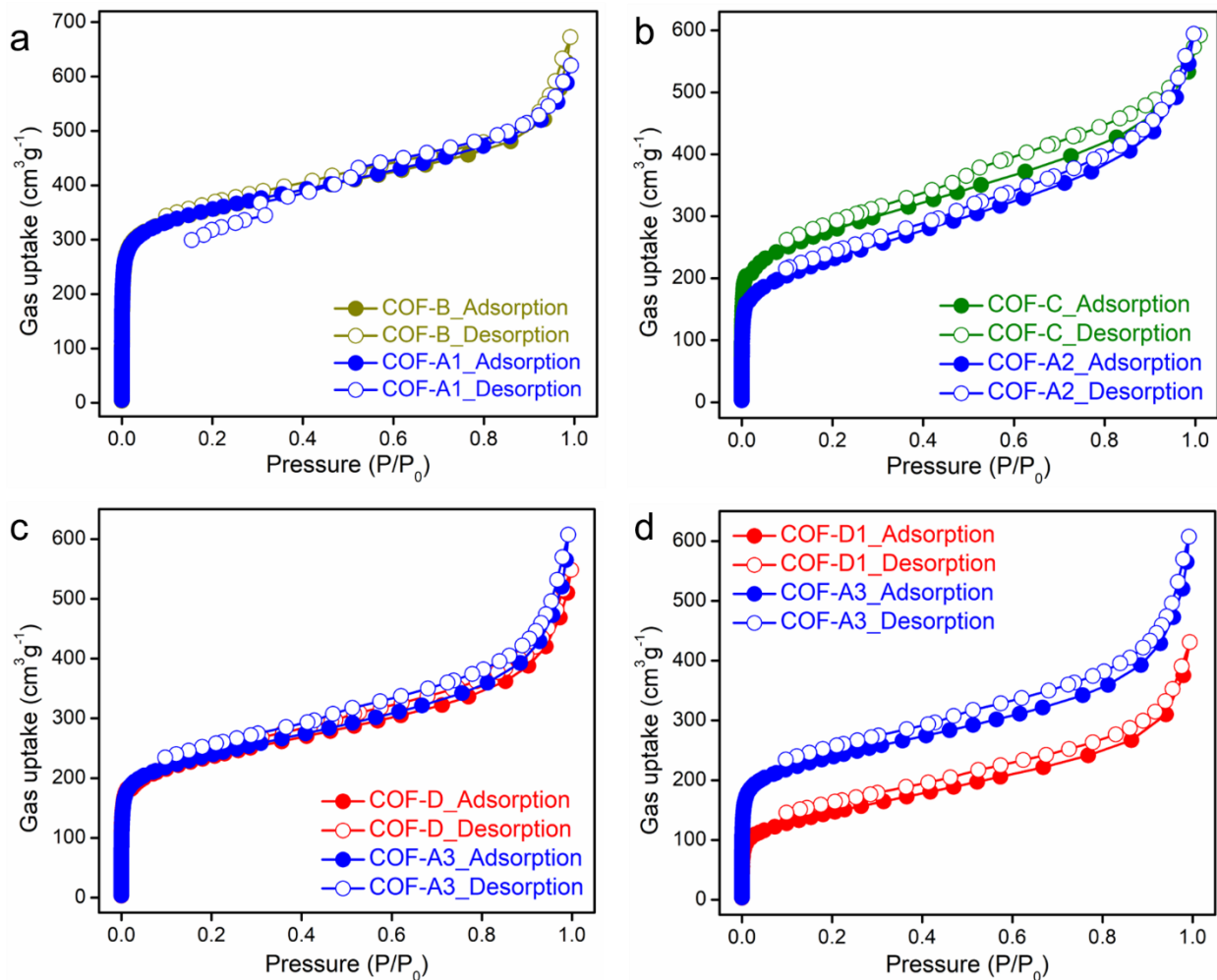


Figure-S35: N₂ gas sorption data at 77 K of (a) COF-A1 and COF-B, (b) COF-A2 and COF-C, (c) COF-A3 and COF-D, and (d) COF-D1 and COF-A3.

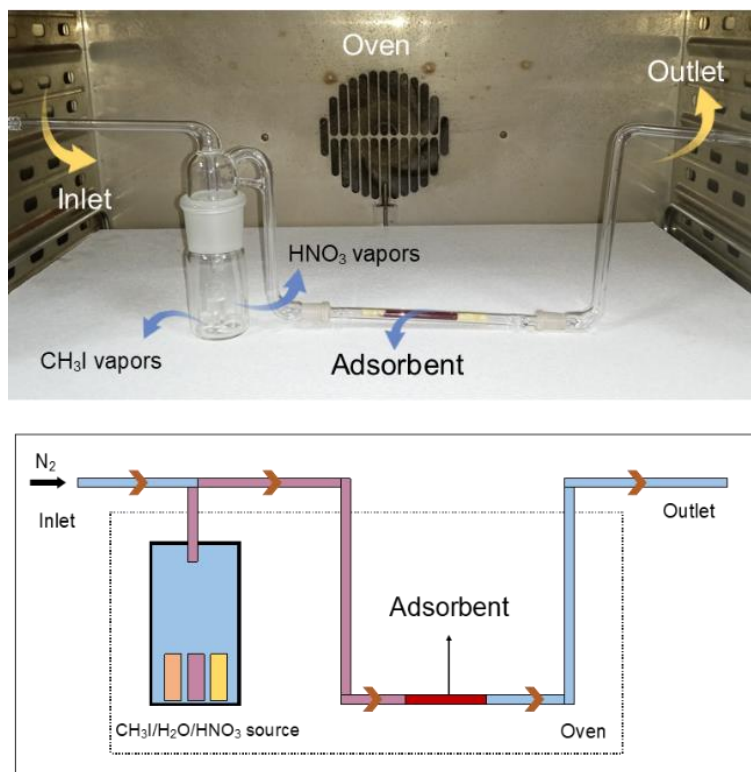


Figure-S36: Digital image and schematic diagram of experimental setup for vapor phase dynamic CH_3I capture test.

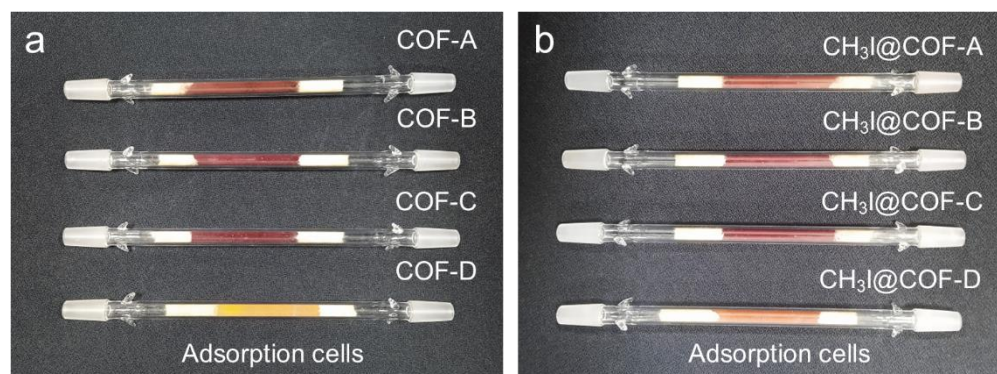


Figure-S37: Images of glass columns packed with COFs (a) before and (b) after adsorption of CH_3I .

Section S8: Post CH₃I adsorption characterizations.

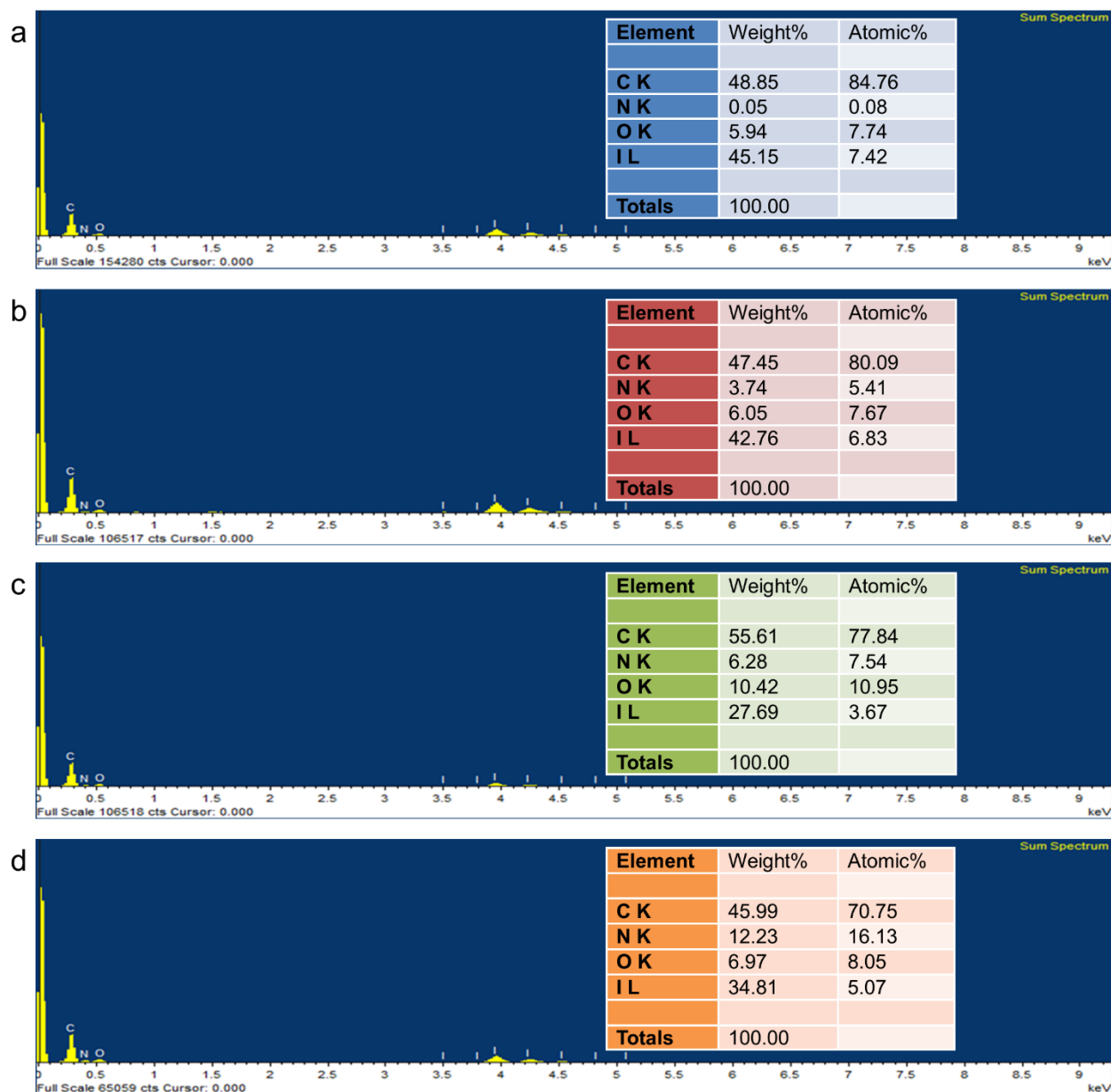


Figure-S38: Energy-dispersive X-ray spectroscopy (EDS) data from FESEM experiment of (a) CH₃I@COF-A, (b) CH₃I@COF-B, (c) CH₃I@COF-C, and (d) CH₃I@COF-D.

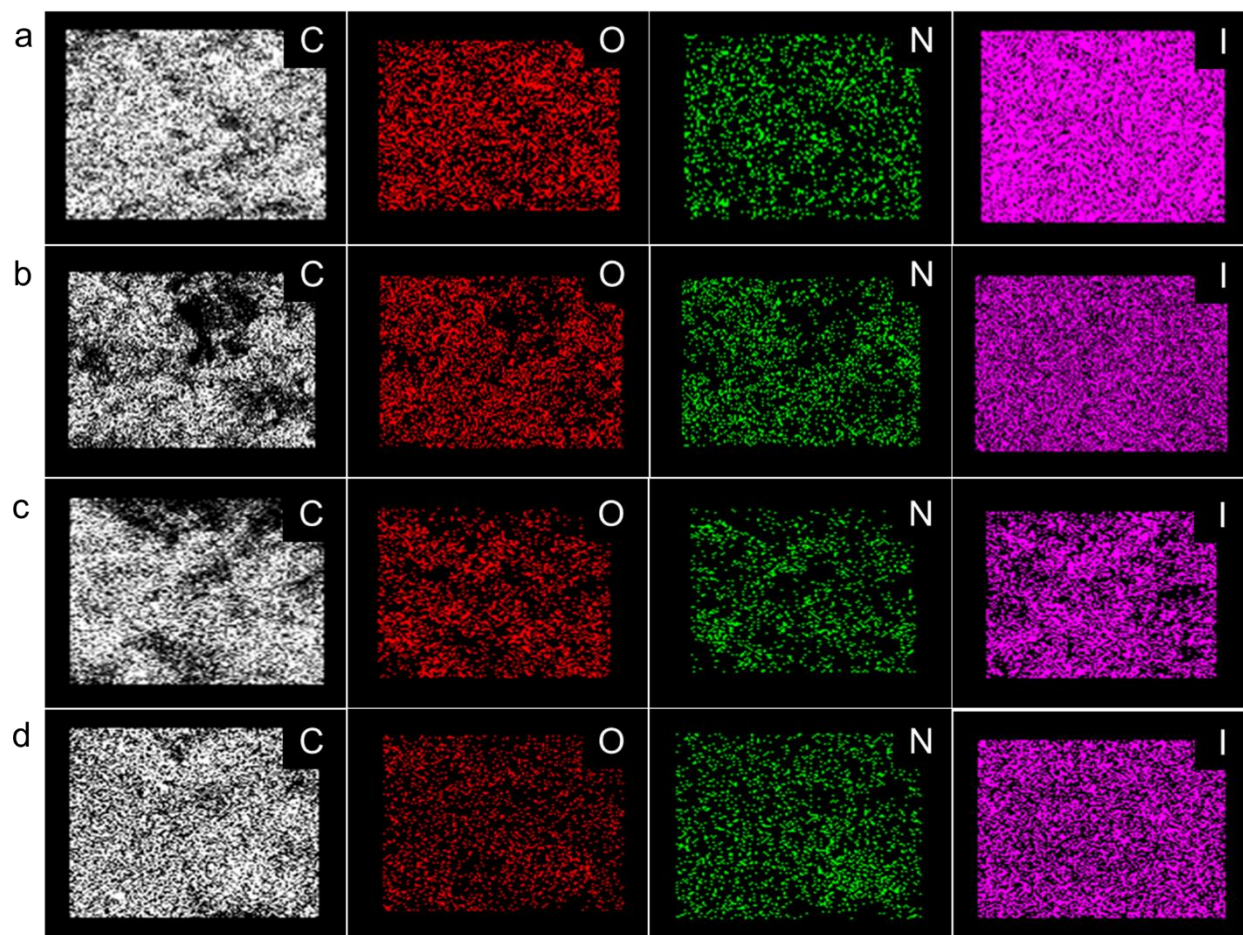


Figure-S39: Elemental mapping images from FESEM experiment of (a) CH₃I@COF-A, (b) CH₃I@COF-B, (c) CH₃I@COF-C, and (d) CH₃I@COF-D.



Figure-S40: Energy-dispersive X-ray spectroscopy (EDS) data from FESEM experiment of (a) CH₃CH₂I@COF-A, (b) CH₃CH₂I@COF-B, (c) CH₃CH₂I@COF-C, and (d) CH₃CH₂I@COF-D.

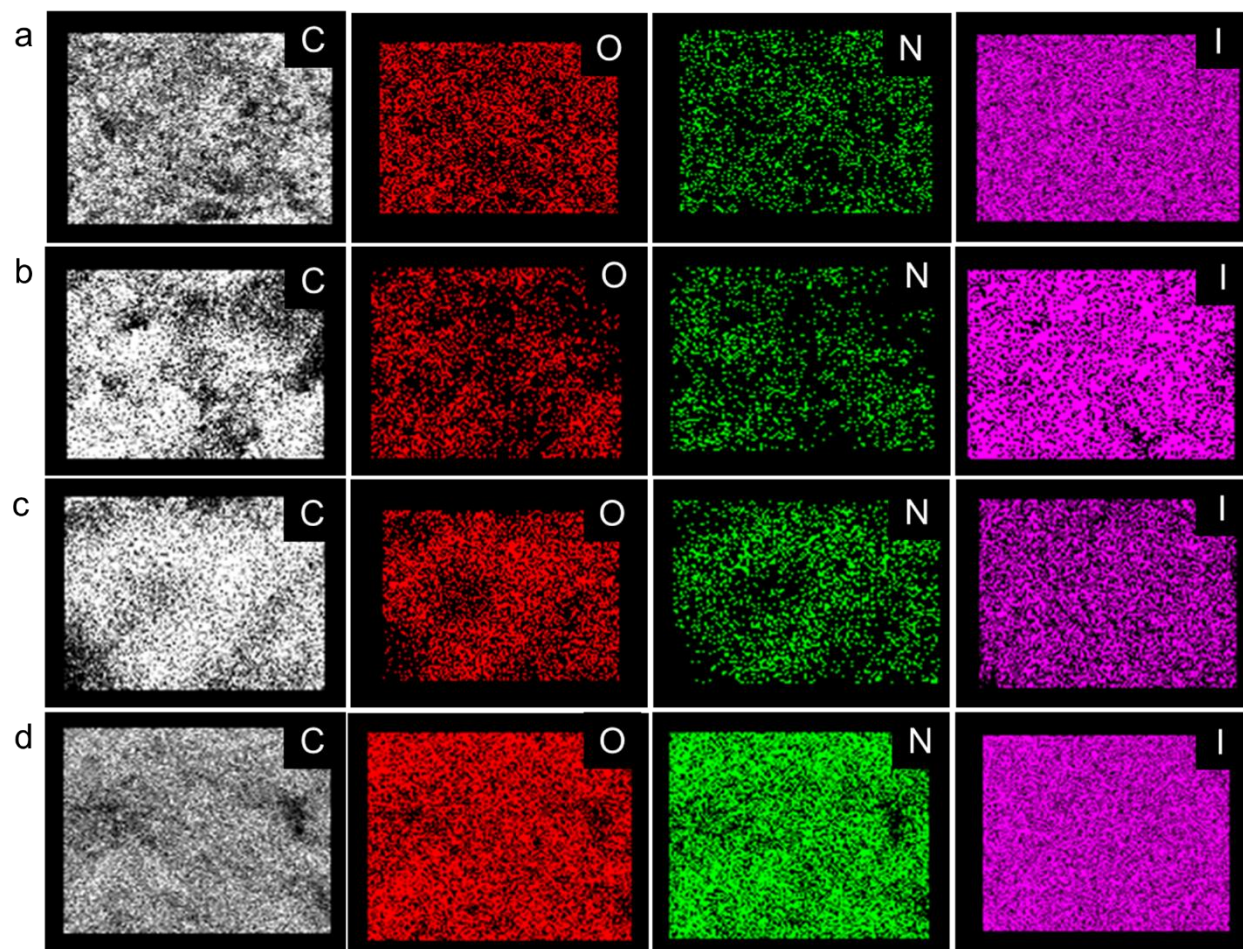


Figure-S41: Elemental mapping images from FESEM experiment of (a) $\text{CH}_3\text{CH}_2\text{I}@$ COF-A, (b) $\text{CH}_3\text{CH}_2\text{I}@$ COF-B, (c) $\text{CH}_3\text{CH}_2\text{I}@$ COF-C, and (d) $\text{CH}_3\text{CH}_2\text{I}@$ COF-D.

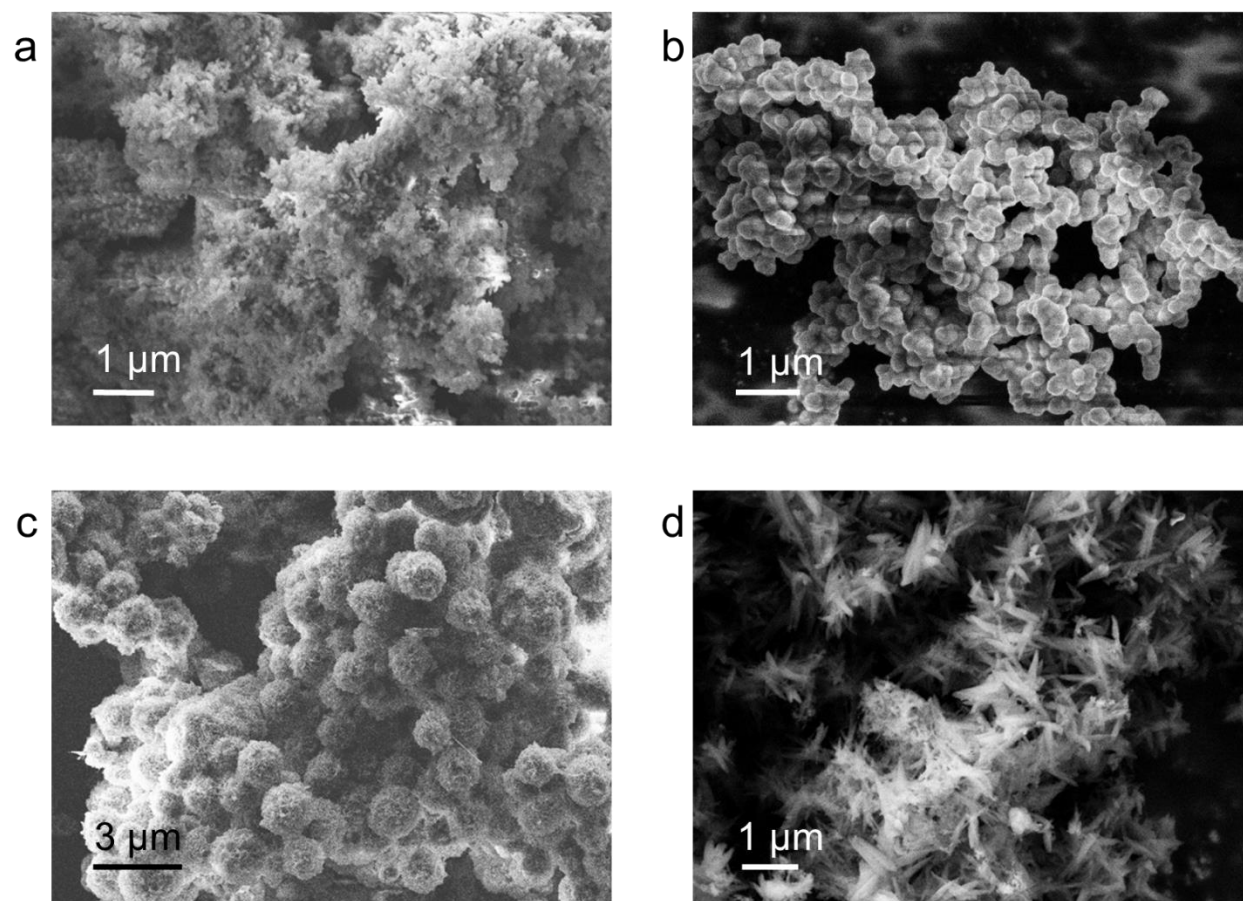


Figure-S42: FESEM images of (a) CH₃I@COF-A, (b) CH₃I@COF-B, (c) CH₃I@COF-C, and (d) CH₃I@COF-D.

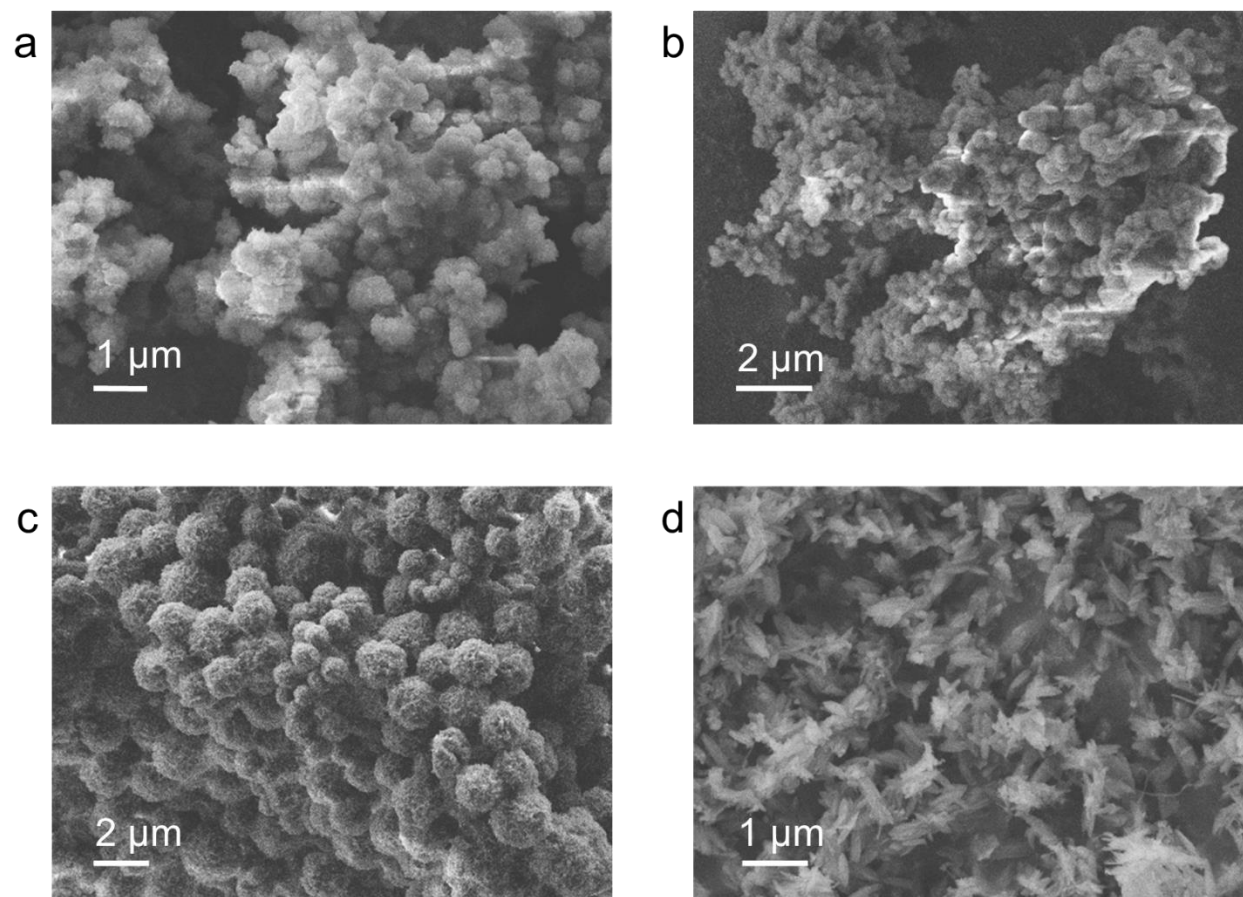


Figure-S43: FESEM images of (a) $\text{CH}_3\text{CH}_2\text{I}@ \text{COF-A}$, (b) $\text{CH}_3\text{CH}_2\text{I}@ \text{COF-B}$, (c) $\text{CH}_3\text{CH}_2\text{I}@ \text{COF-C}$, and (d) $\text{CH}_3\text{CH}_2\text{I}@ \text{COF-D}$.

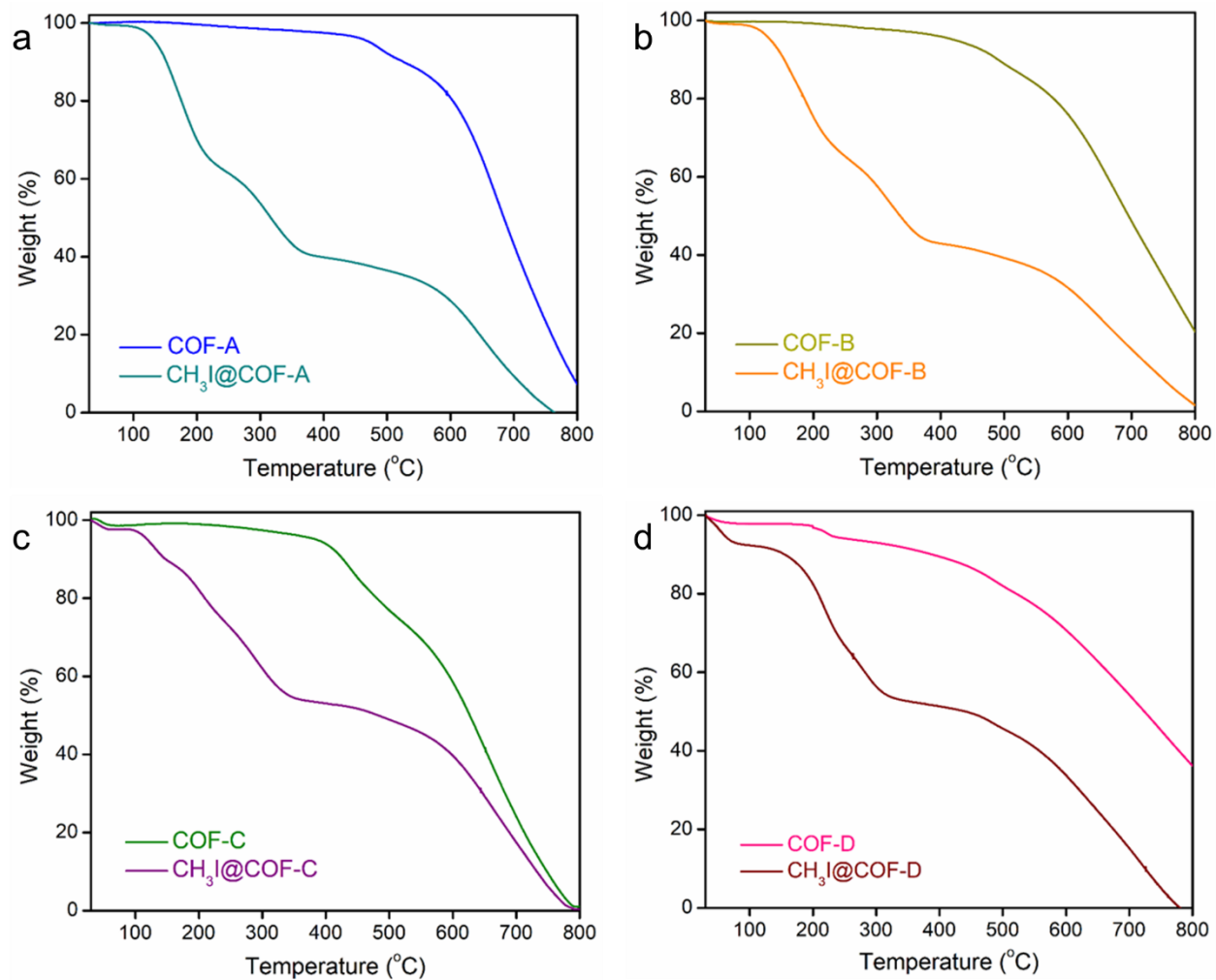


Figure-S44: TGA profiles of (a) CH_3I @COF-A, (b) CH_3I @COF-B, (c) CH_3I @COF-C, and (d) CH_3I @COF-D.

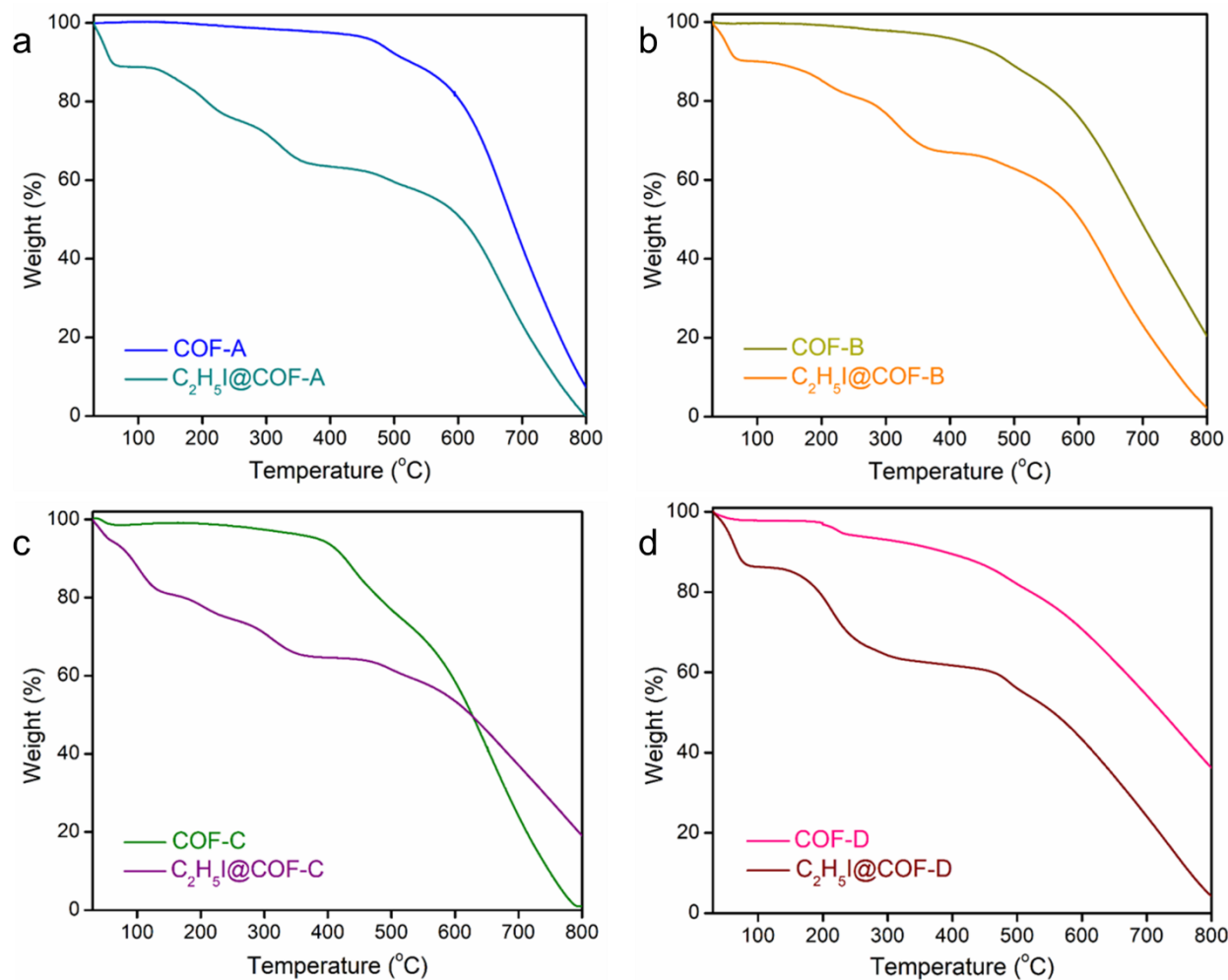


Figure-S45: TGA profiles of (a) CH₃CH₂I@COF-A, (b) CH₃CH₂I@COF-B, (c) CH₃CH₂I@COF-C, and (d) CH₃CH₂I@COF-D.

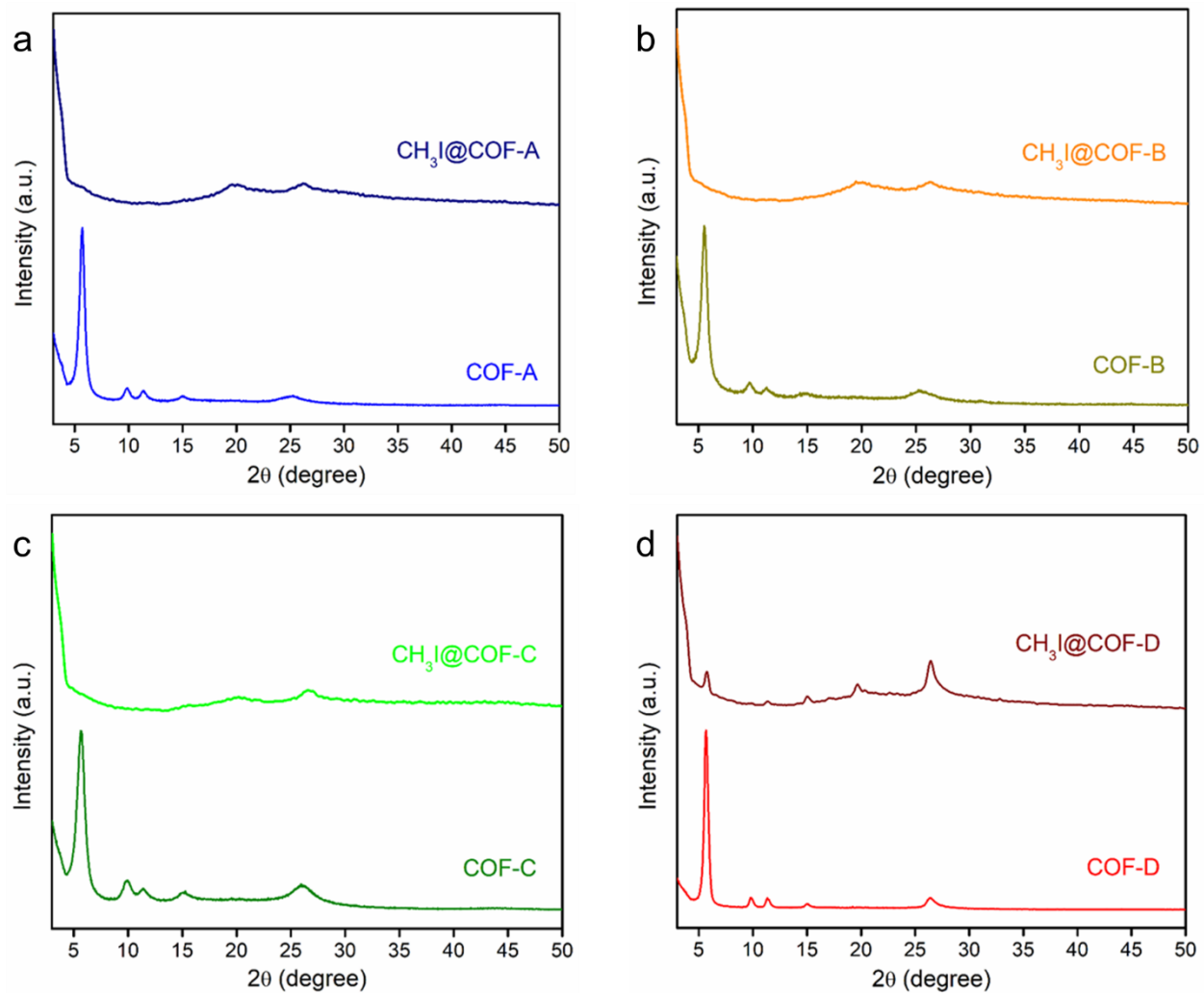


Figure-S46: PXR D patterns of (a) CH₃I@COF-A, (b) CH₃I@COF-B, (c) CH₃I@COF-C, and (d) CH₃I@COF-D.

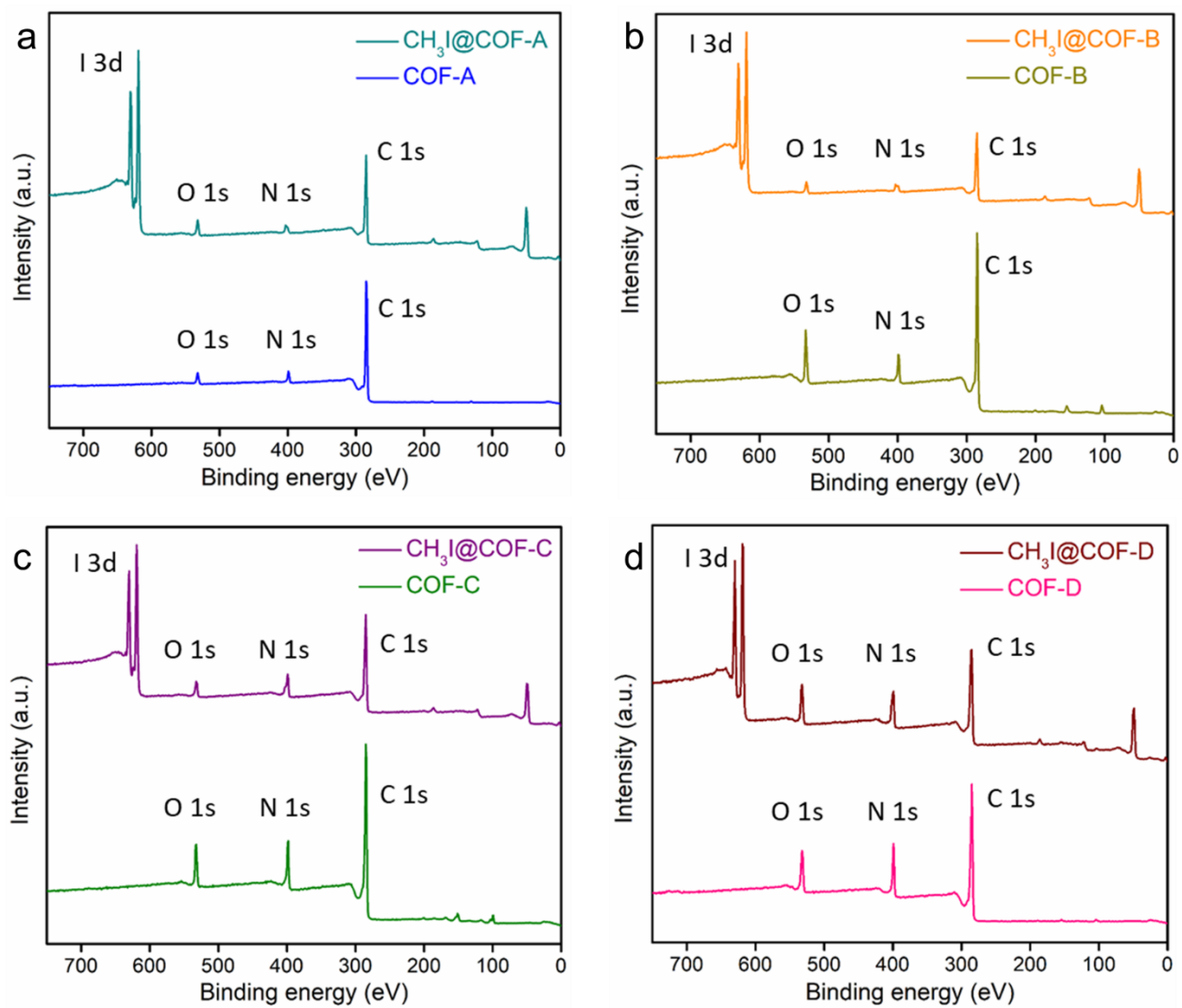


Figure-S47: XPS survey spectra of (a) CH₃I@COF-A, (b) CH₃I@COF-B, (c) CH₃I@COF-C, and (d) CH₃I@COF-D.

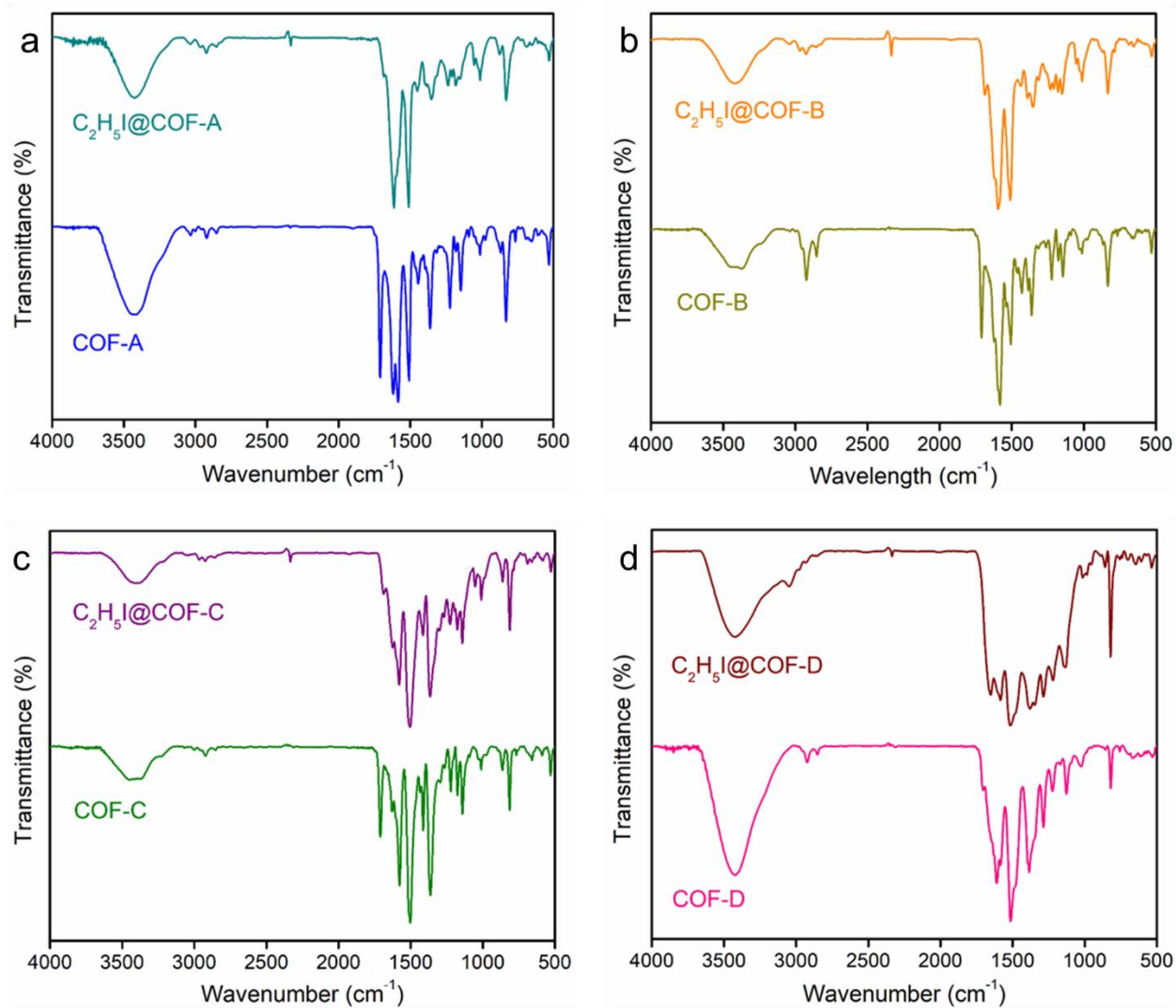


Figure-S48: FTIR spectra of (a) $\text{CH}_3\text{CH}_2\text{I}@$ COF-A, (b) $\text{CH}_3\text{CH}_2\text{I}@$ COF-B, (c) $\text{CH}_3\text{CH}_2\text{I}@$ COF-C, and (d) $\text{CH}_3\text{CH}_2\text{I}@$ COF-D.

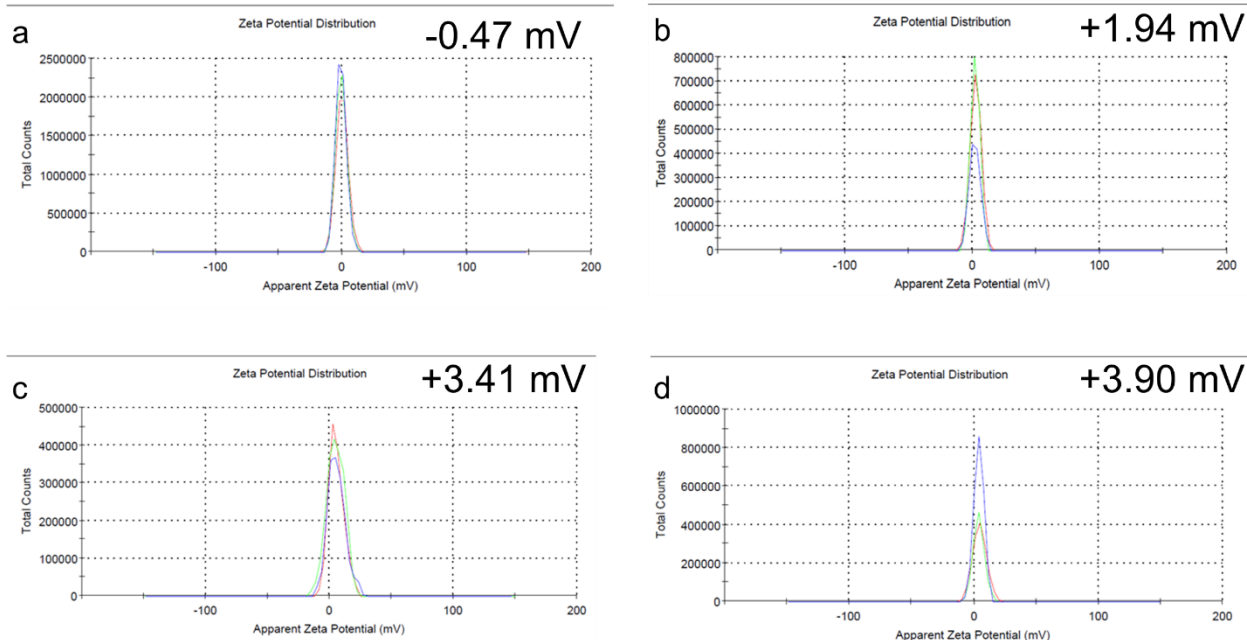


Figure-S49: Zeta potential data of (a) COF-A, (b) COF-B, (c) COF-C, and (d) COF-D.

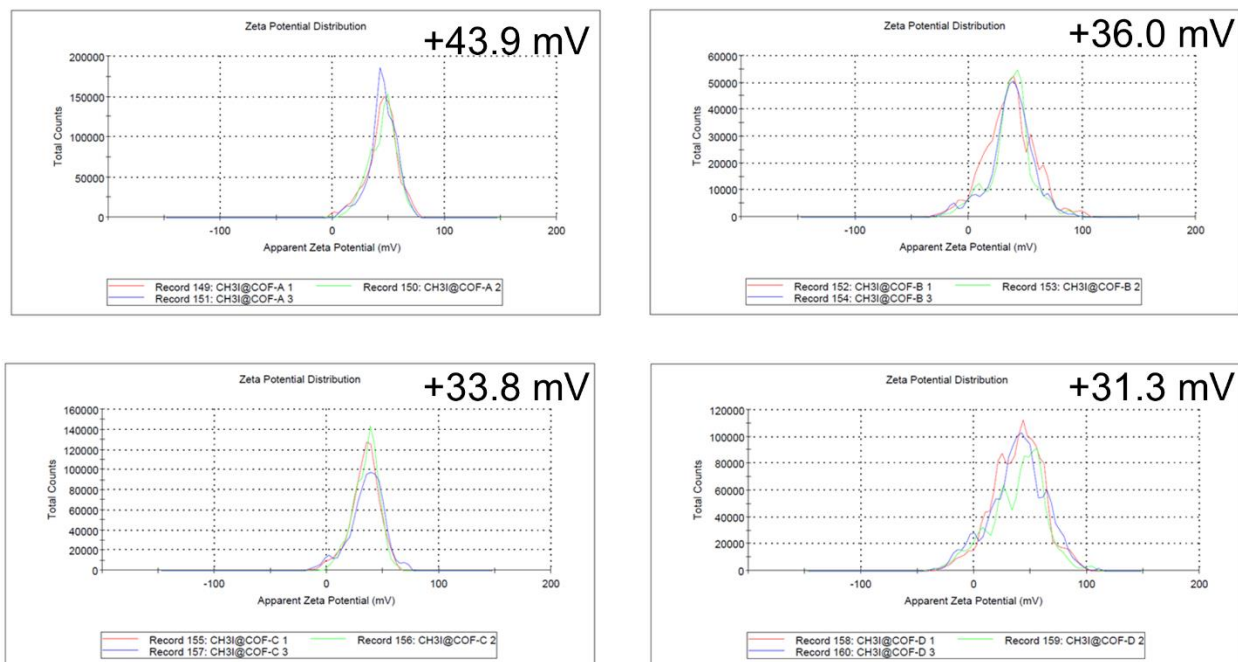


Figure-S50: Zeta potential data of (a) CH₃I@COF-A, (b) CH₃I@COF-B, (c) CH₃I@COF-C, and (d) CH₃I@COF-D.

Section-S9: Organic dye adsorption studies.

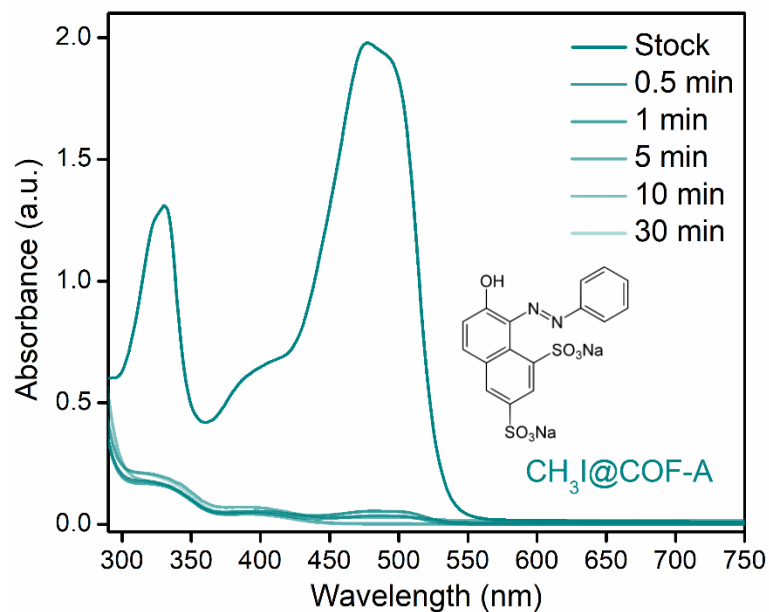


Figure-S51: UV-vis spectra of OG²⁻ dye upon treatment with CH₃I@COF-A.

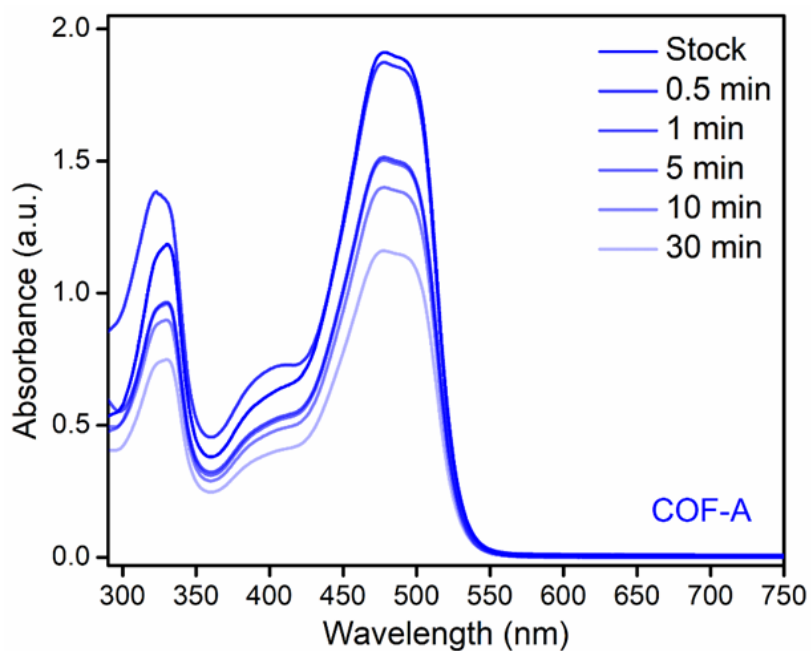


Figure-S52: UV-vis spectra of OG²⁻ dye upon treatment with COF-A.

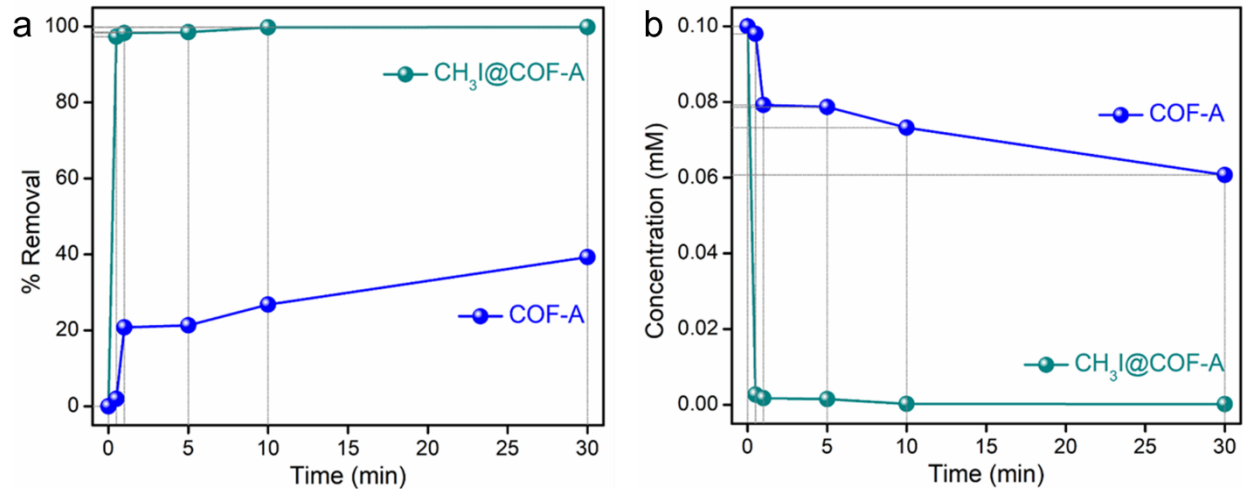


Figure-S53: (a) Removal efficiency and (b) decrease in the concentration of OG²⁻ dye with time upon treatment of CH₃I@COF-A and COF-A.

Note: That being said, in the recent past, ionic porous materials having free exchangeable counter anions were extensively studied for successful sequestration of various contaminants from water. Furthermore, inspired by two independent perspectives, one is the outstanding organic toxics capture performance of the COFs after CH₃I adsorption, and another one is the importance of effective sequestration of organic persistent pollutants towards environmental remediation, we further sought to explore the potential of all CH₃I@COFs towards water treatment application by adsorptive removal of toxic organic dyes from water. Initially, as a typical dye, organic G (OG²⁻) was selected for evaluating the adsorption performances of the as-prepared CH₃I@COFs. The UV-vis spectroscopic analysis was performed to monitor the concentration of the dyes before and after the capture test. As a result, almost ~98%, ~83%, ~62% and ~46% OG²⁻ removal efficiency were observed in case of CH₃I@COF-A, B, C and D, respectively within 30 sec of contact time (Figure-S51-S60). Similar test was performed with pristine COFs, which explored relatively very sluggish OG²⁻ removal kinetics as the UV-vis spectra showed no significant changes in the intensity after the capture test (Figure-S52-S60). The removal efficiency or decrease in the concentration with respect to time profile of all the pristine COFs displayed only ~21%, ~7%, ~6% and ~4% removal efficiency towards OG²⁻ dye capture (Figure-S53, S60). Moreover, these dye adsorption results of the pristine COFs and after CH₃I adsorption were found to follow pseudo-second-order kinetics model with rate constant 1.048, 0.339, 0.151 and

0.0405 g.mg⁻¹.min⁻¹, for CH₃I@COF-A, B, C and D, respectively, towards OG²⁻ pollutant (Figure-S61). Whereas, the rate constant for COF-A, B, C and D were calculated as 0.0229, 0.0193, 0.0302 and 0.0213 g.mg⁻¹.min⁻¹, respectively (Figure-S62). All these findings indicated CH₃I loaded COFs, owing to their cationic charged surface demonstrated significant potential in the improved pollutants sequestration performance (Figure-S63). In addition, with compared to all, CH₃I@COF-A exhibited as the most promising candidate for the ultrafast removal of organic dye (OG²⁻) in water (Figure-S64).

Further, motivated by such excellent enrichment index towards OG²⁻ dye adsorption, the sorption performance of CH₃I@COF-A for other anionic dyes including alizarin red S (ARS), indigo carmine (IC) and methyl orange (MO) were also investigated. In a similar typical capture test, the UV-vis spectra of these dyes exhibited rapid diminishing of intensities with respect to time when treated with CH₃I@COF-A (Figure-S65). Interestingly, very fast kinetics of capture was observed in all the cases with the equilibrium reaching within less than 1 min. These results indicated excellent potency of CH₃I@COF-A in the effective adsorption of anionic dyes (OG, ARS, IC, and MO) in water medium, which was also associated with a distinct color change of the dye solutions visible to the naked eye (Figure-S66, S67). The ultrafast adsorption of anionic dyes by CH₃I@COF-A emphasize the fact that electrostatic interactions with Coulombic attractions are the significant prevailing factor in trapping these molecules.

Next, the ability of CH₃I@COF-A to successfully and effectively adsorb anionic dyes owing to its cationic nature motivated us to investigate its selectivity based on charge specificity. For this we conducted the similar capture test with a cationic dye, methylene blue (MB) in water. CH₃I@COF-A exhibited negligible adsorption ability towards MB even after treatment of 30 min (Figure-S68). Additionally, a binary dye mixture-based adsorption investigation using dye molecules that were both cationic and anionic was conducted. CH₃I@COF-A was subjected to an equimolar combination of 1 mL anionic MO and 1 mL cationic MB in order to observe the adsorption behavior by UV-vis spectroscopy. Notice that under identical experimental circumstances, almost ~98% removal efficiency of the anionic MO dye was observed, whereas, only ~7% of the cationic methylene blue was removed, (Figure-S69). These findings support the electrostatic interactions' predominance in determining the contaminants' adsorption efficiency and the selective character of CH₃I@COF-A (Figure-S70). The color shift seen throughout the experiment provided more evidence of the selective adsorption behavior. After attaining equilibrium, the color of the mixed binary dye solution progressively shifted from green to blue, indicating the predominance of non-adsorbed methylene blue in the leftover stock solution (Figure-S70).

Further, a crucial consideration when assessing an adsorbent for practical applications is its column extraction ability. Therefore, it was also looked into whether CH₃I@COF-A was conceptually feasible for wastewater cleanup in real-time applications. We developed a fixed-bed stationary-phase column-based experimental setup to put this into practice (Figure-

S71). In this typical experiment, a stock OG^{2-} dye solution was passed through a bed of $\text{CH}_3\text{I@COF-A}$ with a flow rate of $0.5 \text{ mL}\cdot\text{min}^{-1}$, and the column eluent solution was analyzed using UV-visible analysis (Figure-S72). As a result of breakthrough test, almost $\sim 55 \text{ mL}$ of outflow solution, OG^{2-} dye removal efficiency was over 93% (Figure-S73). After which, the C/C_0 ratio was gradually increased until complete adsorbent saturation after $\sim 107 \text{ mL}$ of column eluent. This result showed the remarkable dynamic capture efficiencies of the adsorbent towards real-time waste-water treatment.

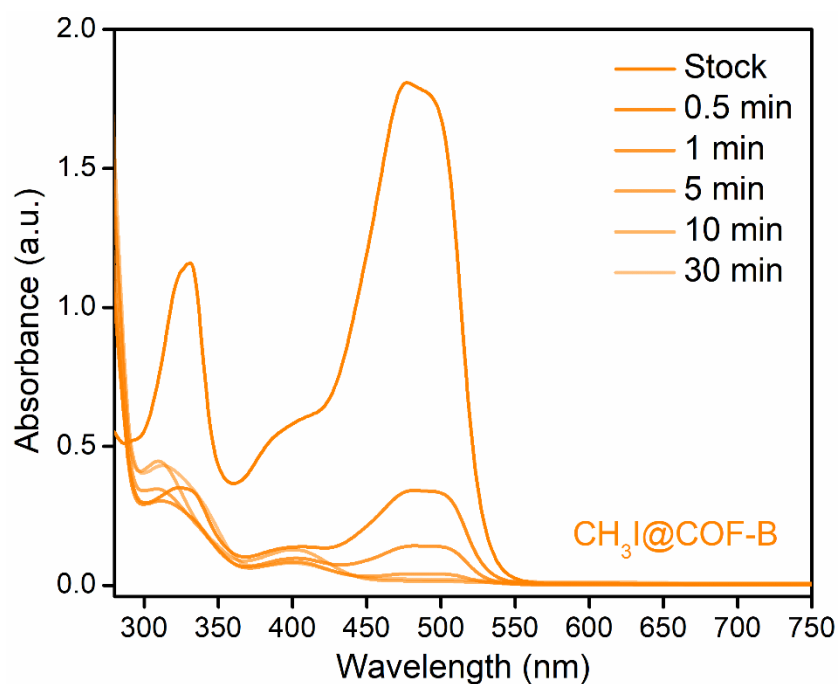


Figure-S54: UV-vis spectra of OG^{2-} dye upon treatment with $\text{CH}_3\text{I@COF-B}$.

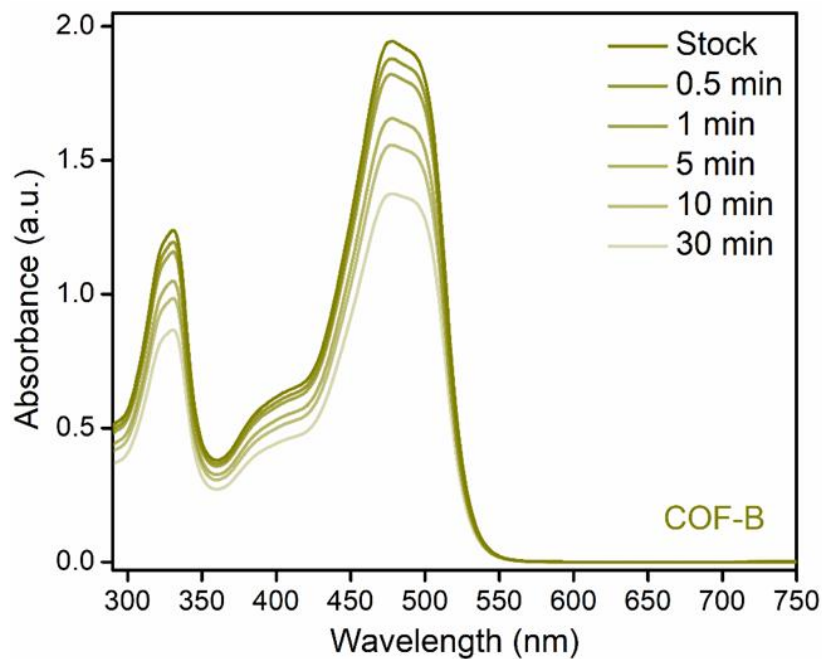


Figure-S55: UV-vis spectra of OG^{2-} dye upon treatment with COF-B.

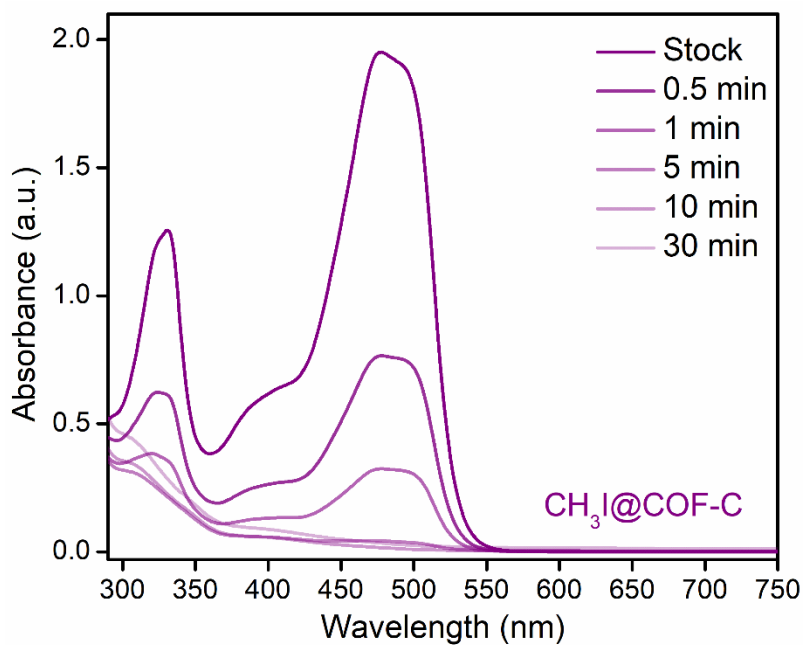


Figure-S56: UV-vis spectra of OG^{2-} dye upon treatment with $\text{CH}_3\text{I}@$ COF-C.

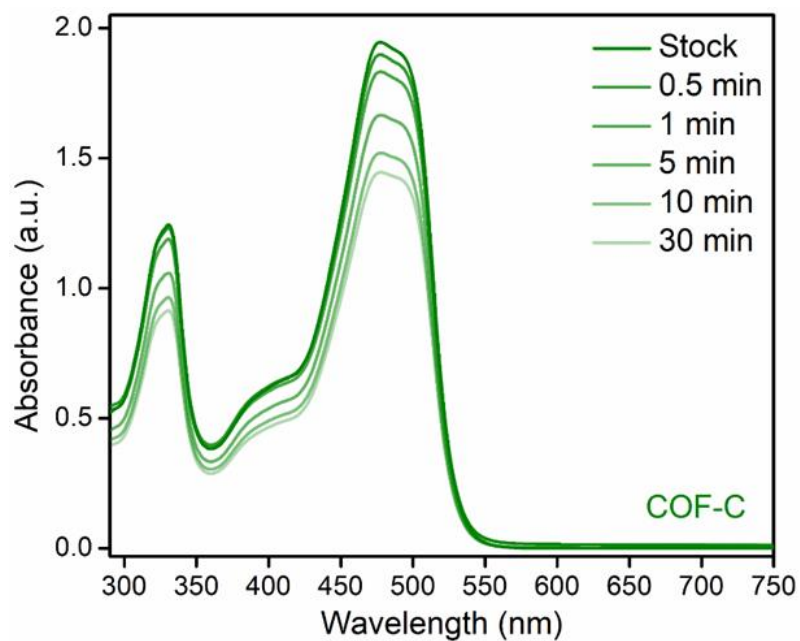


Figure-S57: UV-vis spectra of OG²⁻ dye upon treatment with COF-C.

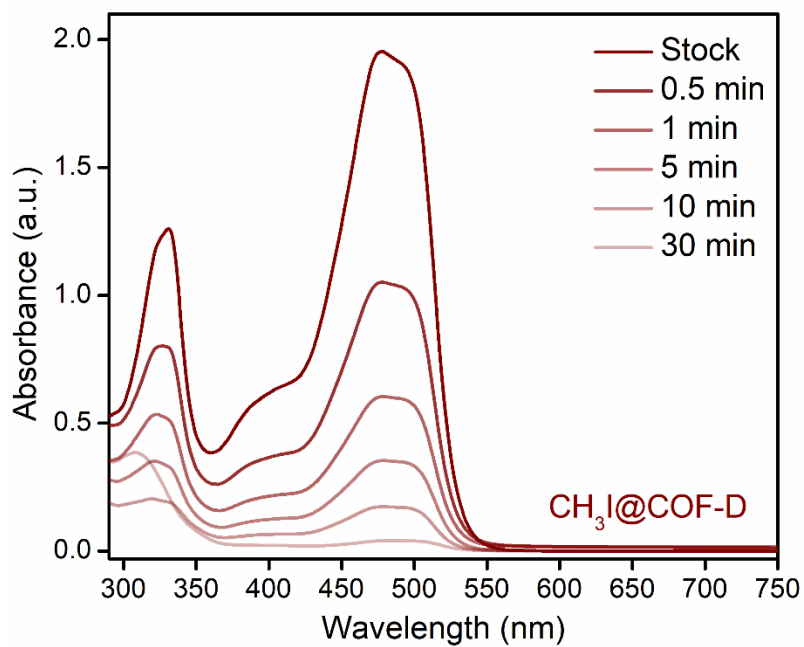


Figure-S58: UV-vis spectra of OG²⁻ dye upon treatment with CH₃I@COF-D.

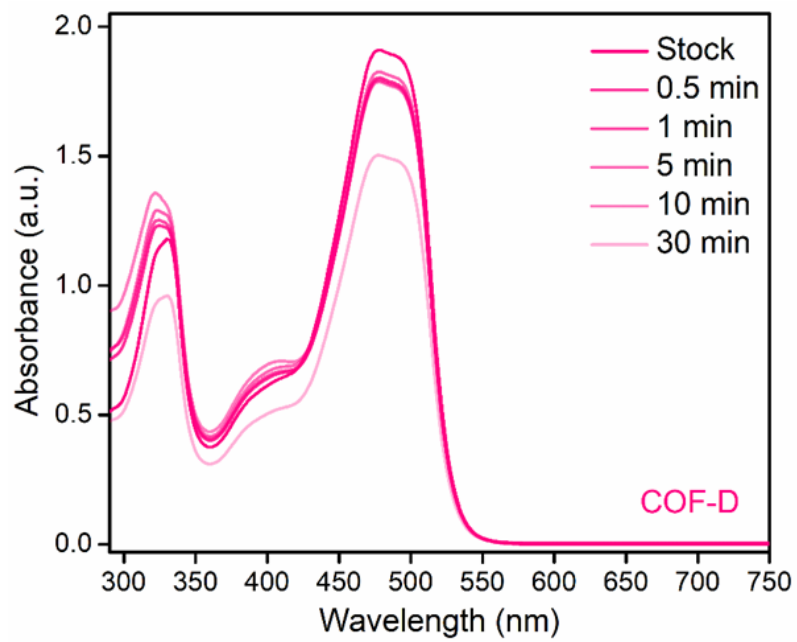


Figure-S59: UV-vis spectra of OG²⁻ dye upon treatment with COF-D.

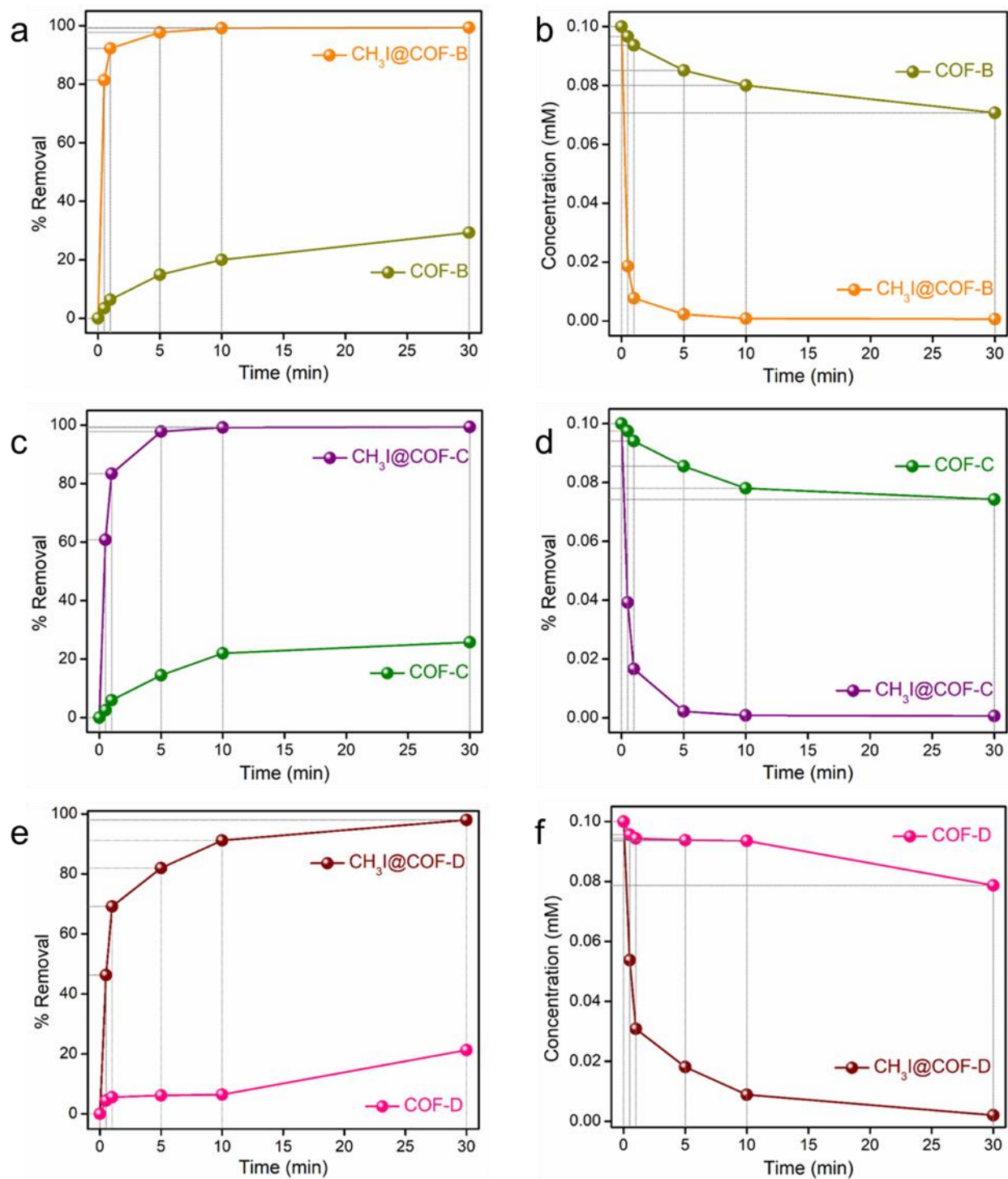


Figure-S60: (a, c, e) Removal efficiency and (b, d, f) decrease in the concentration of OG²⁻ dye with time upon treatment of CH₃I@COF-B and COF-B, CH₃I@COF-C and COF-C, and CH₃I@COF-D and COF-D, respectively.

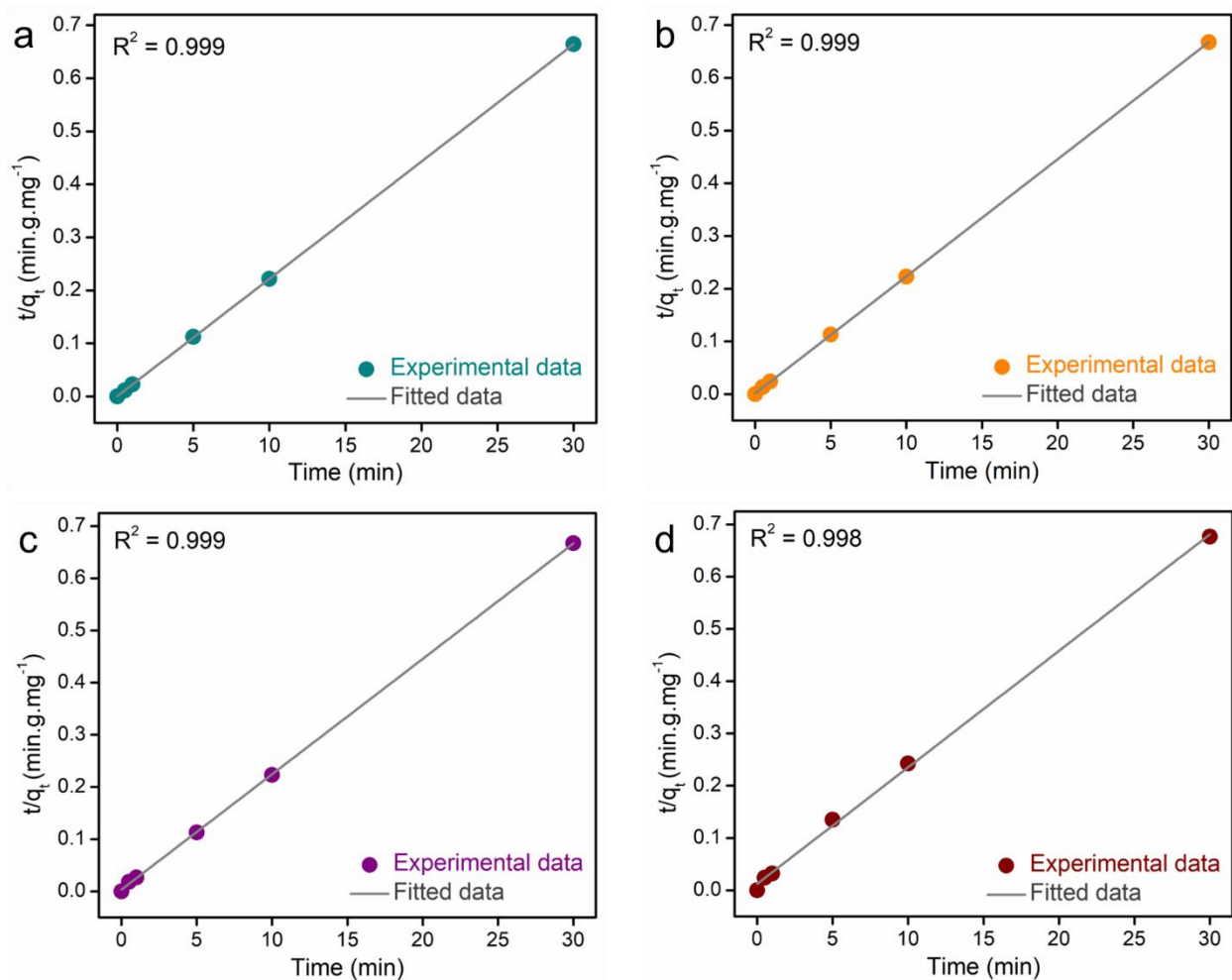


Figure-S61: Pseudo-second-order model fitting of adsorption of OG²⁻ dye by (a) CH₃I@COF-A, (b) CH₃I@COF-B, (c) CH₃I@COF-C, and (d) CH₃I@COF-D.

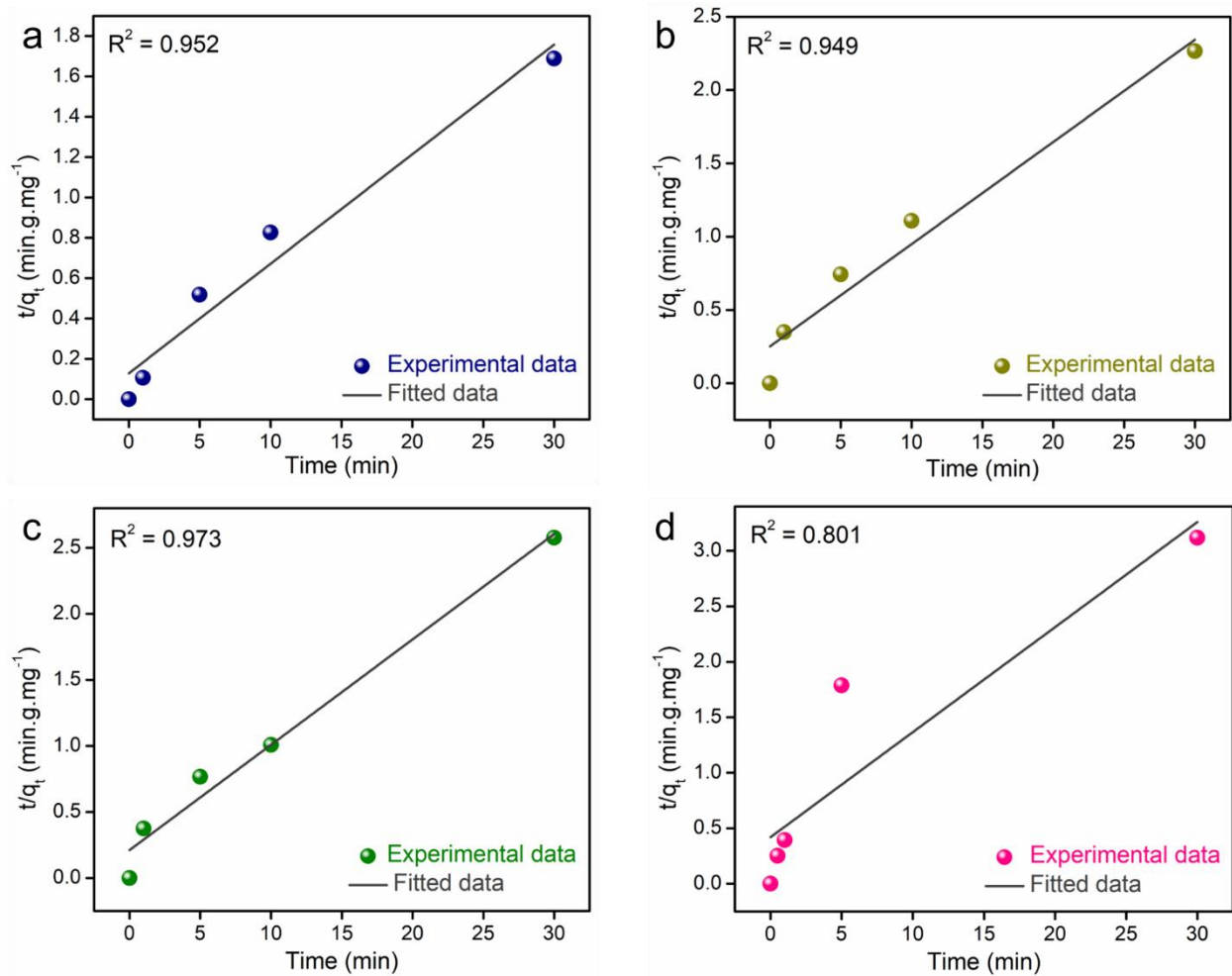


Figure-S62: Pseudo-second-order model fitting of adsorption of OG²⁻ dye by (a) COF-A, (b) COF-B, (c) COF-C, and (d) COF-D.

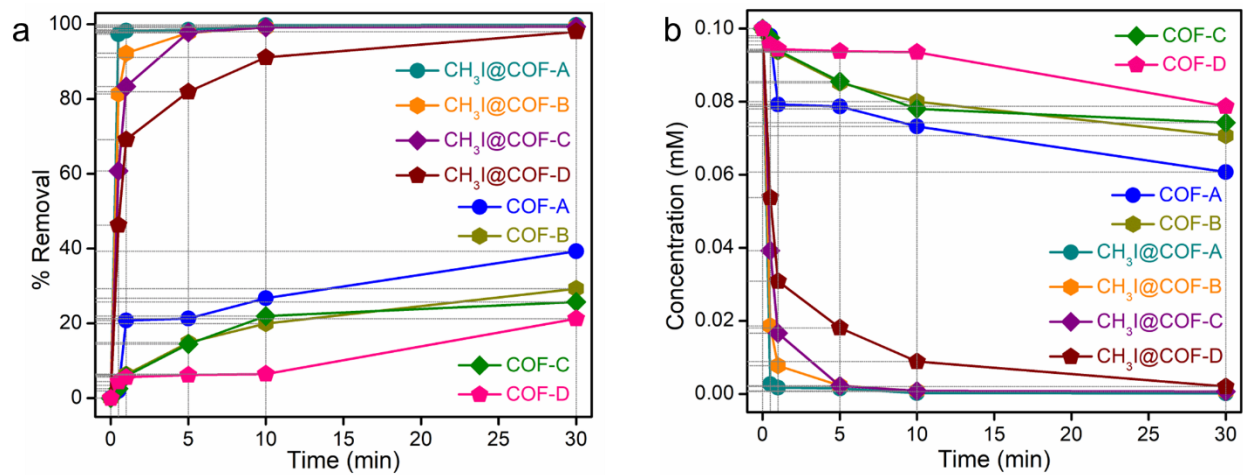


Figure-S63: (a) Removal efficiency and decrease in the concentration of OG^{2-} dye with time upon treatment of $\text{CH}_3\text{I}@$ COF-A and COF-A, $\text{CH}_3\text{I}@$ COF-B and COF-B, $\text{CH}_3\text{I}@$ COF-C and COF-C, and $\text{CH}_3\text{I}@$ COF-D and COF-D, respectively.

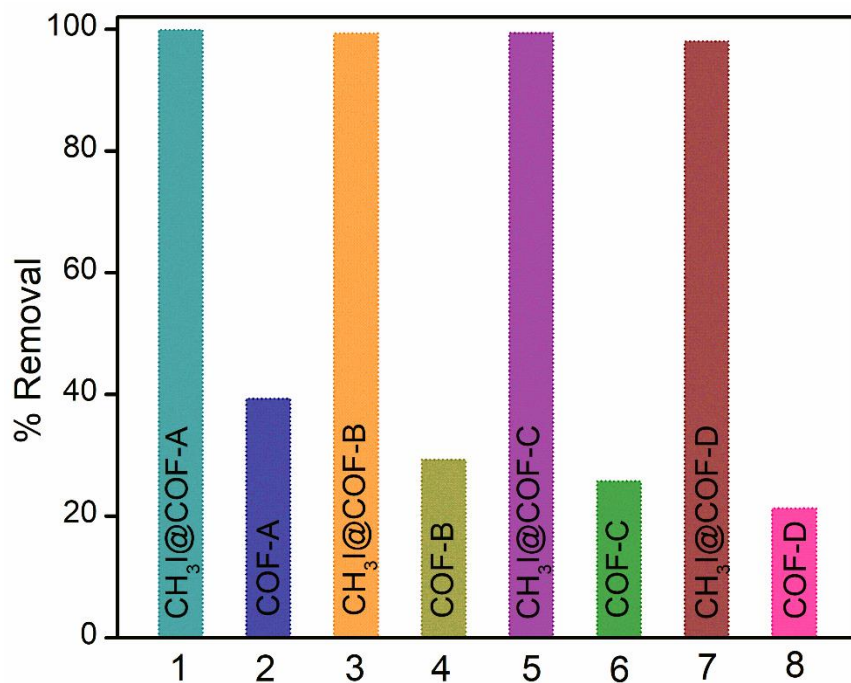


Figure-S64: (a) Removal efficiency of OG^{2-} aqueous solution by COF-A, B, C and D, before and after CH_3I adsorption.

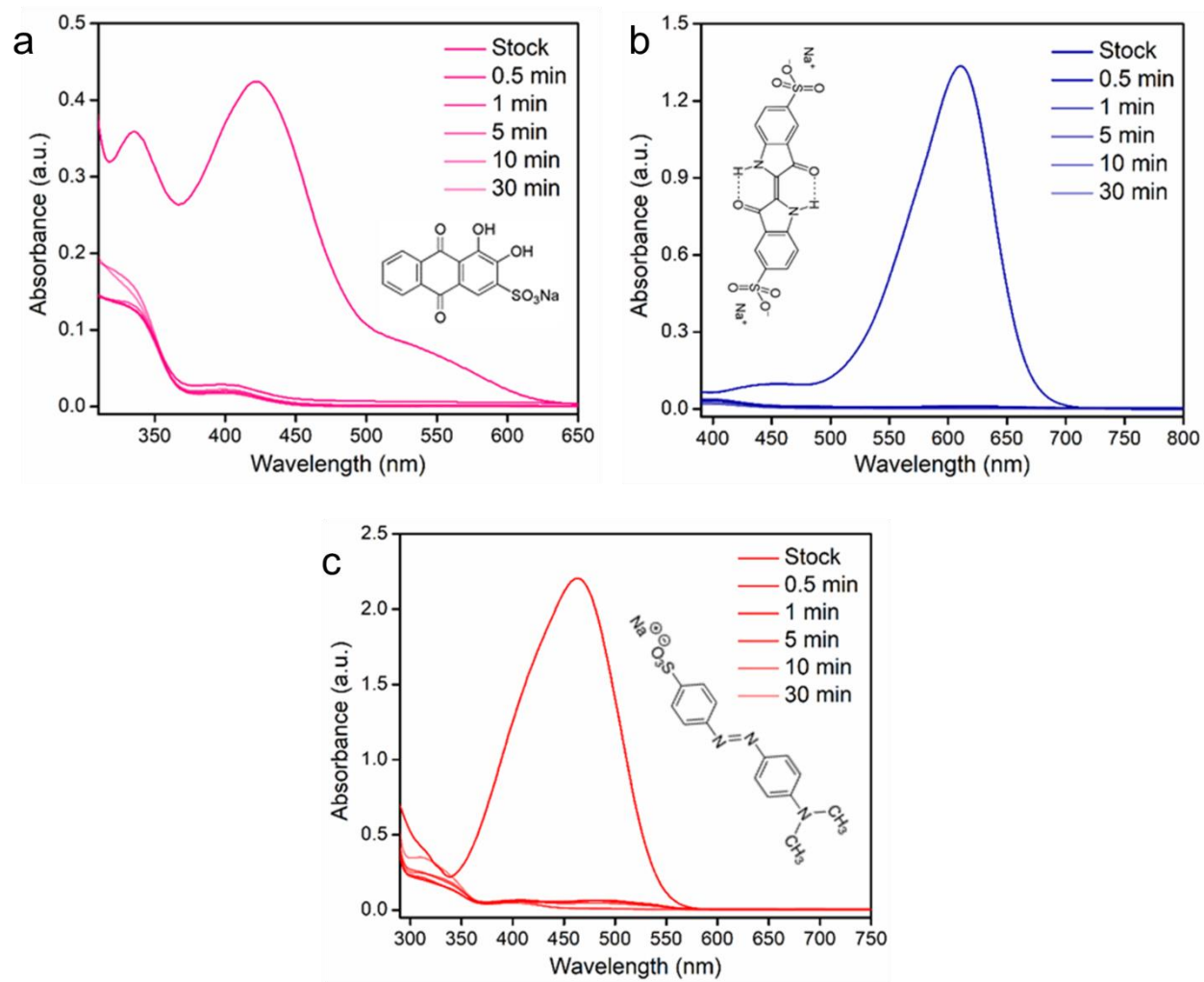


Figure-S65: UV-vis spectra of (a) alizarin red S (ARS), (b) indigo carmine (IC) and (c) methyl orange (MO) dyes upon treatment with $\text{CH}_3\text{I}@\text{COF-A}$.

Dye	Stock	0.5 min	1 min	5 min	10 min	30 min	60 min	
OG								---
IC								---
ARS								---

Figure-S66: Digital images of change in the colors of (a) orange G (OG), (b) indigo carmine (IC) and (c) alizarin red S (ARS), dyes with time upon treatment with $\text{CH}_3\text{I}@\text{COF-A}$.

Dye	Stock	0.5 min	1 min	5 min	10 min	30 min	60 min	
MB								MB
MO								---
MO + MB								MB

Figure-S67: Digital images of change in the colors of (a) methylene blue (MB), (b) methyl orange (MO) and (c) mixture of MB and MO, dyes with time upon treatment with $\text{CH}_3\text{I}@\text{COF-A}$.

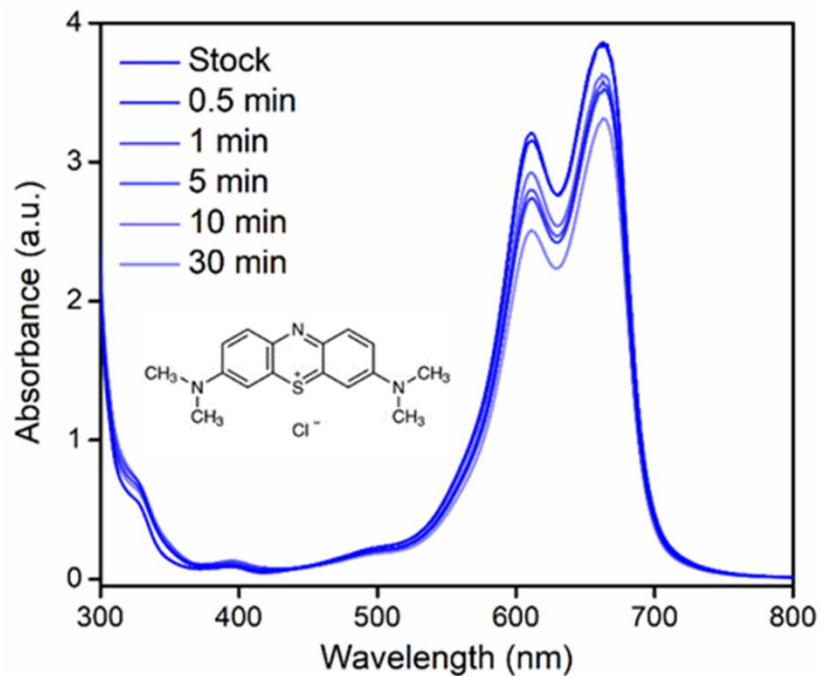


Figure-S68: UV-vis spectra of methylene blue (MB) dyes upon treatment with CH₃I@COF-A.

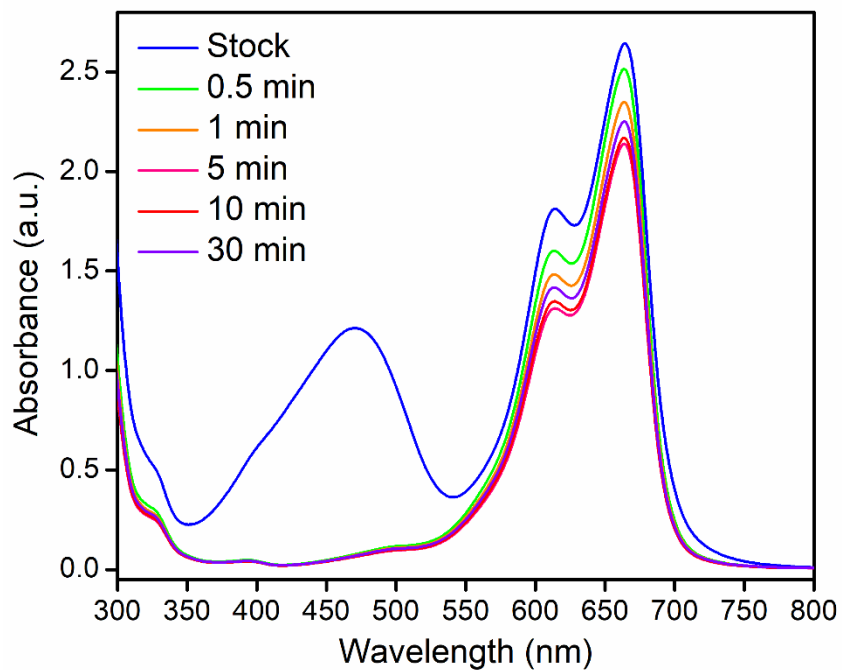


Figure-S69: UV-vis absorption spectra for the selective adsorption of MO from the binary mixture of MO-MB in water by CH₃I@COF-A.

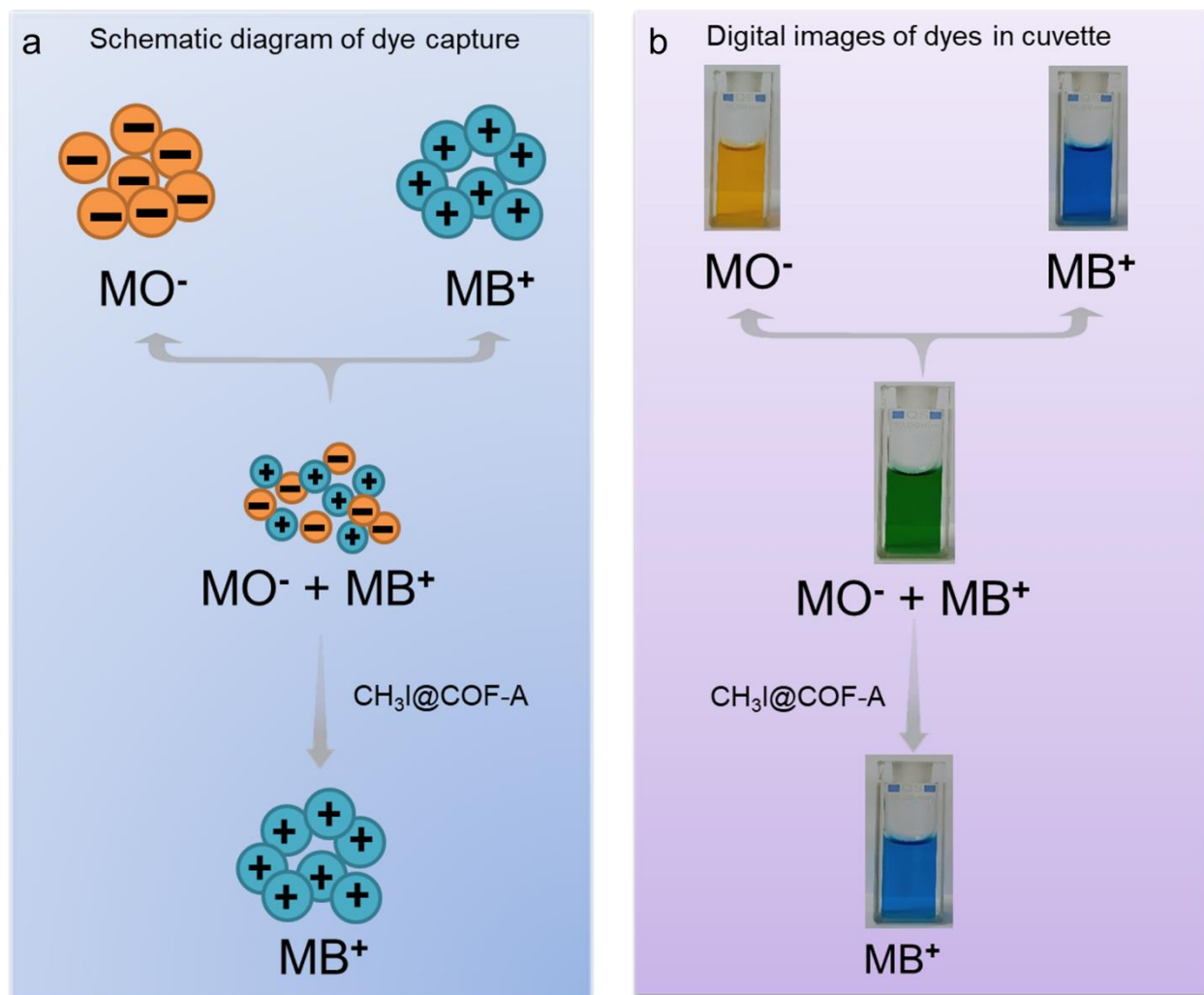


Figure-S70: (a) Schematic diagram and (b) images of selective capture of anionic MO dye over cationic MB dye in a binary mix dye capture test.

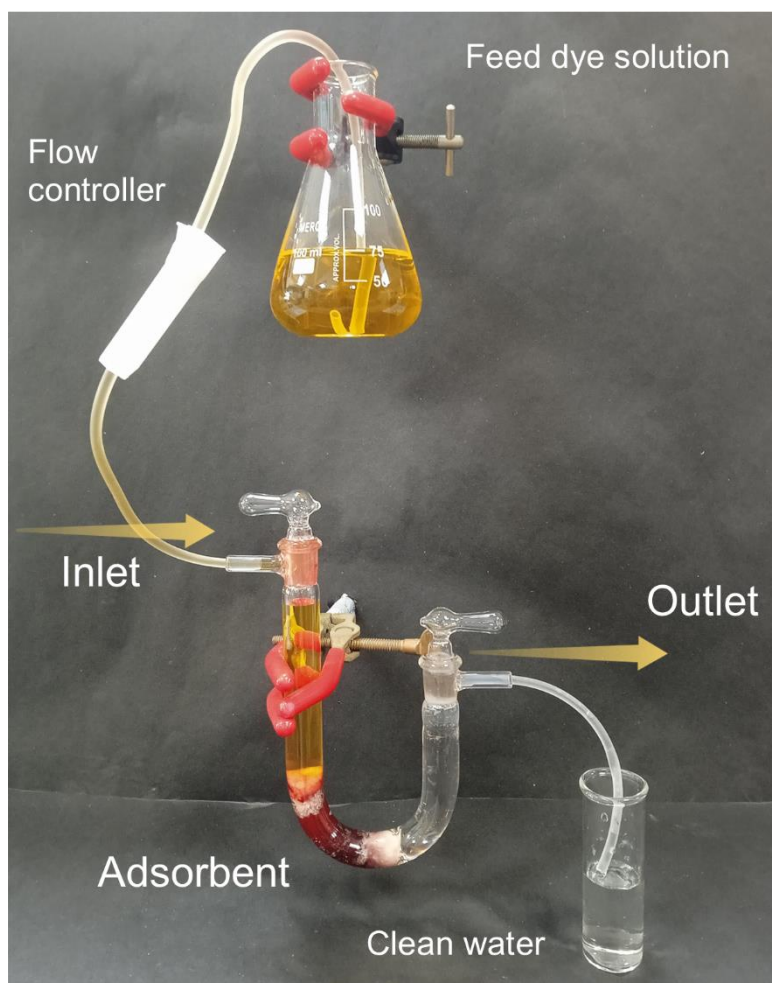


Figure-S71: Digital image of $\text{CH}_3\text{I}@\text{COF-A}$ based column setup for dynamic flow-through OG^{2-} dye capture test.

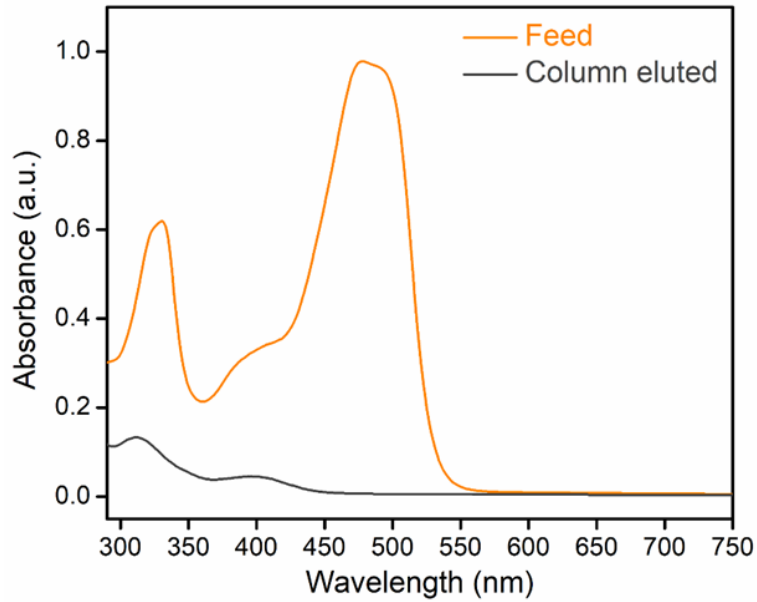


Figure-S72: UV-vis spectra of OG^{2-} dye upon treatment with $\text{CH}_3\text{I}@\text{COF-A}$ based fixed bed column.

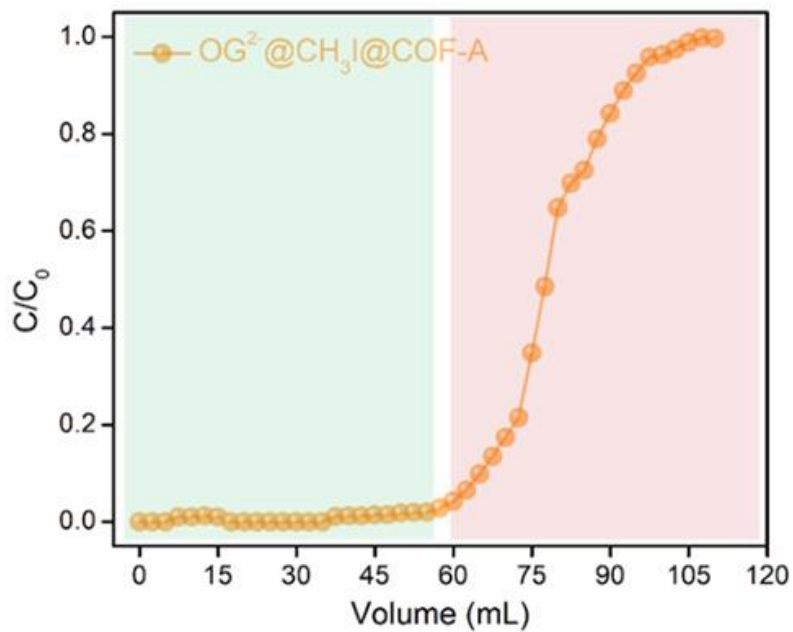


Figure-S73: Breakthrough profile of dynamic column based OG^{2-} capture test by $\text{CH}_3\text{I}@\text{COF-A}$.

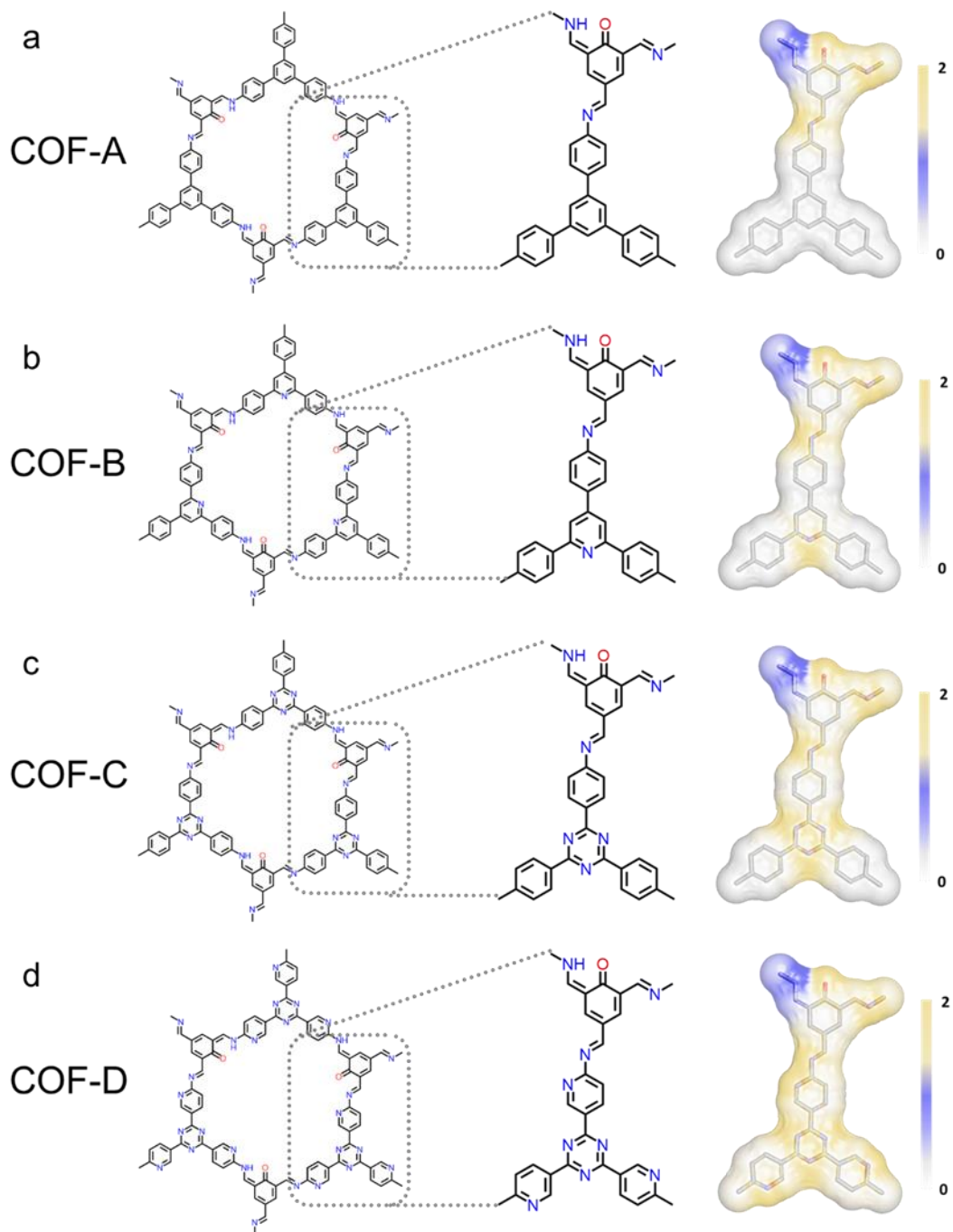


Figure-S74: Repeating units of the COFs as the model molecules to represent the structures of (a) COF-A, (b) COF-B, (c) COF-C, and (d) COF-D.

Section S10: References

- [1] G. H. Ning, Z. Chen, Q. Gao, W. Tang, Z. Chen, C. Liu, B. Tian, X. Li and K. P. Loh, *J. Am. Chem. Soc.* 2017, **139**, 8897–8904.
- [2] W. Chen, W. Yan, S. Wu, Z. Xu, K. W. K. Yeung and C. Yi, *Macromol. Chem. Phys.* 2010, **211**, 1803–1813.
- [3] R. Gomes, P. Bhanja and A. Bhaumik, *Chem. Commun.*, 2015, **51**, 10050-10053.
- [4] S. Haldar, R. Kushwaha, R. Maity and R. Vaidhyanathan, *ACS Mater Lett.* 2019, **1**, 490–497.
- [5] D. Chakraborty, S. Nandi, D. Mullangi, S. Haldar, C. P. Vinod and R. Vaidhyanathan, *ACS Appl Mater Interfaces* 2019, **11**, 15670–15679.
- [6] S. Ruidas, A. Das, S. Kumar, S. Dalapati, U. Manna and A. Bhaumik, *Angew. Chem. Int. Ed.* 2022, **61**, e202210507.
- [7] Y. Xie, T. Pan, Q. Lei, C. Chen, X. Dong, Y. Yuan, W. A. Maksoud, L. Zhao, L. Cavallo, I. Pinnau and Y. Han, *Nat. Commun.* 2022, **13**, 2878.